INTERNATIONAL ATOMIC ENERGY AGENCY
UNITED NATIONS EDUCATIONAL, SCIENTIFIC AND CULTURAL ORGANIZATION

INTERNATIONAL CENTRE FOR THEORETICAL PHYSICS
34100 TRIESTE (ITALY) - P.O.B. 586 - MIRAMARE - STRADA COSTIERA 11 - TELEPHONE: 2240-1
CABLE: CENTRATOM - TELEX 460392-I

H4.SMR/285 - 5

WINTER COLLEGE ON
LASER PHYSICS: SEMICONDUCTOR LASERS
AND INTEGRATED OPTICS

(22 February - 11 March 1988)

OPTICAL SEMICONDUCTOR DEVICES

B. Mroziewicz
Institute of Electron Technology
Warsaw, Poland

OPTICAL SEMICONDUCTOR DEVICES

Bohdan MROZIEWICZ

Institute of Electron Technology
Warsaw, Poland

December 1987

Prepared for ICTP

OUTLINE

INTRODUCTION

The purpose of this lecture is to give a review of the most important optical semiconductor devices with the priority assigned to semiconductor lasers and detectors used as sensors of the laser radiation. Therefore the infrared devices will be mostly exposed with only marginal attention paid to those operating in the visible region of the spectrum.

General features of the above mentioned devices which are considered essential to their applications will be discussed and comparisons whenever possible will be made in order to illustrate the state-of-the art in the field. Devices employed in fibre optic communication systems will be treated more in detail since progress in this technique is still a driving force for the whole present optoelectronics.

Because of the large variety of design and materials existing in the technology of both semiconductor emitters and detectors an attempt will be made to show some general ideas or trends that have been implemented in practice. Classification of these designs will be made to allow the reader to make his own selection of the classes of the devices that might be of interest to him in his future studies. For that purpose each chapter of the lecture will be provided with the bibliography selected as the most relevant for the subject.

1. GENERAL CONSIDERATIONS

Operation of all optical semiconductor devices is based on two fundamental optical processes: photon absorption and radiative recombination leading to photon emission.

Accordingly, optical semiconductor devices can be classified into two basic groups: detectors and emitters. They are employed to convert flux of optical energy or optical signals into electrical current and vice versa. In many applications emitters and detectors are used as optically coupled source/detector systems. If assembled together in a common housing such devices are called optocouplers. When the optical coupling is achieved with an optical fibre the system becomes a fibre optic link.

Considering both construction of the optical semiconductor devices and their applications, the whole family of these devices can be visualized as shown in Fig.1.1.

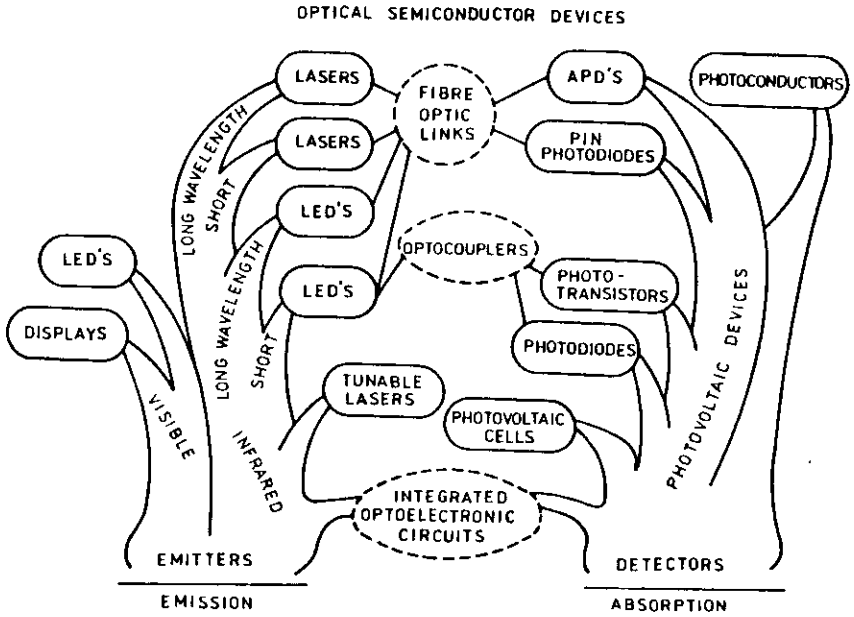

Fig.1.1. Optical semiconductor devices form now a large device family. Their operation is based on the two physical processes: Emission and Absorption

Optical radiation is understood to mean electromagnetic radiation in the range of wavelengths between 10 nm and 1 mm. The optical radiation band consists of the subranges UV (Ultra-violet), visible radiation (Light) and IR (Infra-red). The range of the optical spectrum covered by semiconductor emitters is displayed in Fig.1.2 and Fig.1.3a,b. Analogous graphs can be plotted for semiconductor detectors.

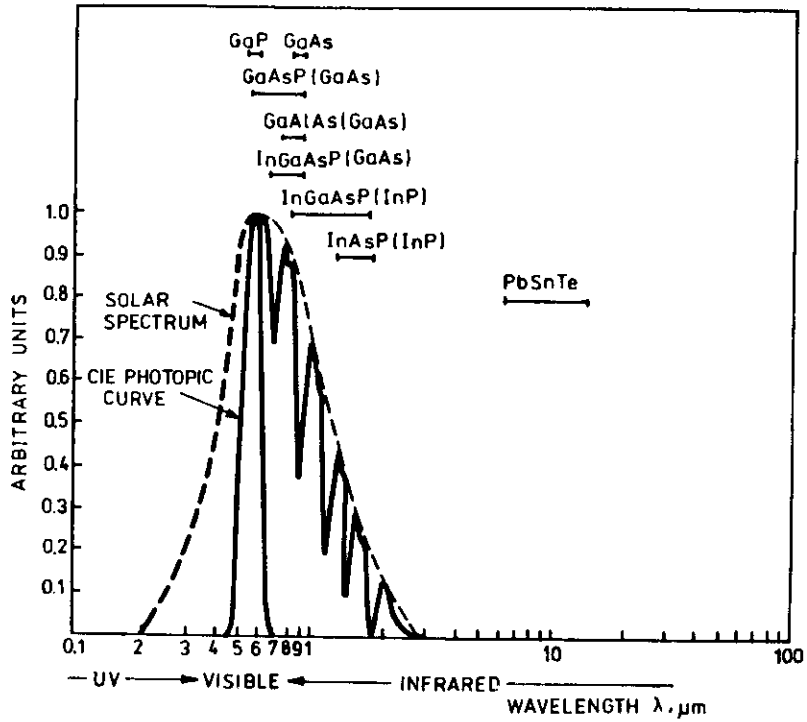

Fig.1.2. Spectral distribution of the currently fabricated semiconductor emitters. The sensitivity of the human eye and solar spectrum are also plotted to show that they occupy only a small part of the optical radiation spectrum

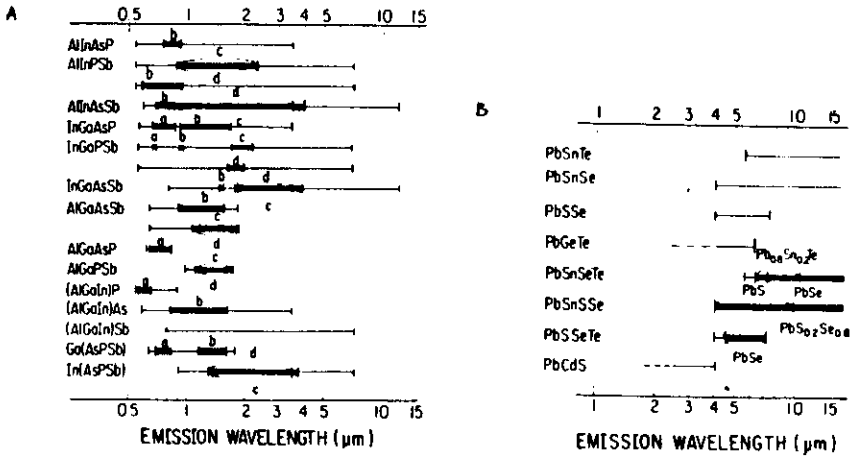

Fig.1.3. Expected emission wavelengths for various III-V quaternaries at 300K(A) and IV - VI mixed crystals at 77K(B). The thick portion in (A) denotes the compositions which are lattice matched to stable binary crystals: (a) GaAs, (b) InP, (c) GaSb, (d) InAs ; shaded areas correspond to the miscibility gaps [1]

It is worthwhile to notice that although the expression "Light" relates only to the optical radiation perceived and evaluated by the human eye, the names of all semiconductor emitters commonly refer to "Light" regardless the wavelength of their emission, like Light Emitting Diodes (LEDS)or Lasers. However, recently this approach seems as being to be changed and in more precise definitions, the term "infrared" appears e.g. IRED.

HISTORICAL OUTLINE

Optical semiconductor devices have over 60 years long history marked by developments of new significant devices. However, the real beginning of the activity in this field is usually bound to invention of junction lasers.

Years

1873 - discovery of the photoconductivity in selenium (W. Smith)

1923 - emission of light observed from p-n junctions naturally occurring in SiC (Lossew)

1952 - first photovoltaic detectors (germanium photovoltaic cells)

1962 - first semiconductor injection lasers

1962 - first germanium and silicon p-i-n photodiodes

1965 - development of silicon avalanche photodiodes

1968 - first commercial LEDs and LED displays

1970 - CW lasing action obtained at room temperature

1974 - 1.3 μm lasers made of InGaAsP/InP heterostructures

1977 - first Quantum Well lasers

Most striking achievements are noted in the field of semiconductor lasers (Figs 1.4 and 1.5).

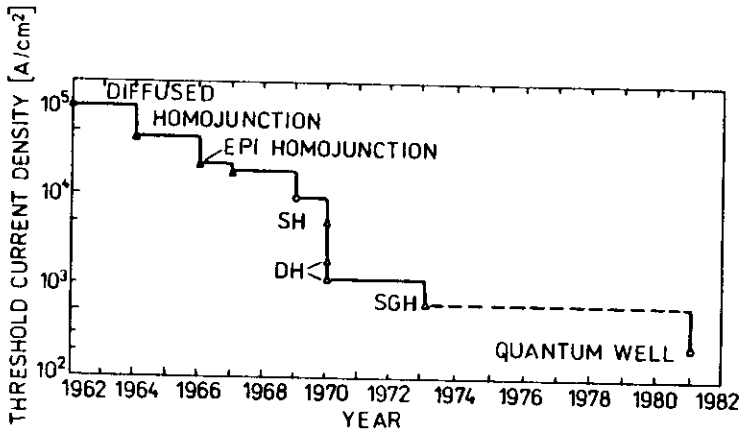

Fig.1.4. Threshold current density of semiconductor lasers has been improved by almost 3 orders of magnitude making these devices applicable in practice

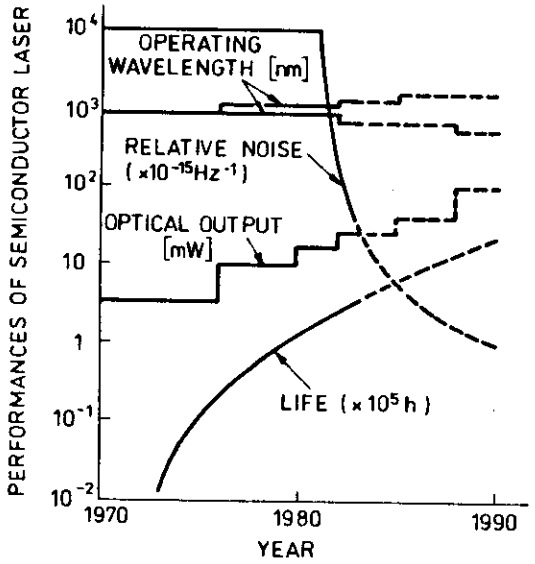

Fig.1.5. Progress of semiconductor lasers and their future prospects. Research and development of semiconductor laser proceeds towards the enlargement of the operating wavelength range, high output power, low noise and long life

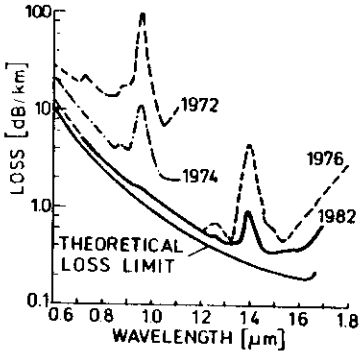

Fig.1.6. Loss spectra of representative multimode fibers (doped silica core), illustrating progress made in the past decade. This progress has been a major driving force for the development of optical semiconductor devices

MAJOR FEATURES OF THE OPTICAL SEMICONDUCTOR DEVICES

EMITTERS

- High power efficiency (up to 50%)
- High speed (up to 15 GHz)
- Wavelength selection
- Narrow spectral linewidth (45 Å for LEDs, 0.01 Å or 300 MHz) AlGaAs/GaAs devices
- Supply voltage compatible with ICs
- Small dimensions of the optical source

- High reliability
- long lifetime ($<10^6$ hrs) small over all dimensions
- Lightweight
- Mechanical ruggedness

DETECTORS

- High quantum efficiency and responsivity (≥ 0.7 A/W)
- High speed (range of nanoseconds)
- Good linearity
- Relalively low noise figure (NEP 4×10^{-15} W/H$^{1/2}$)
- Wide spectral response

OPTOCOUPLERS

- High voltage isolation (up to 10 kV)
- Broad bandwidth
- Supply voltage compatible with ICs

APPLICATIONS OF THE OPTICAL SEMICONDUCTOR DEVICES

visible LEDs and displays: optical indicators

photodetectors (visible range): sensors
measurement systems
solar cells

infrared devices: see Fig.1.7.

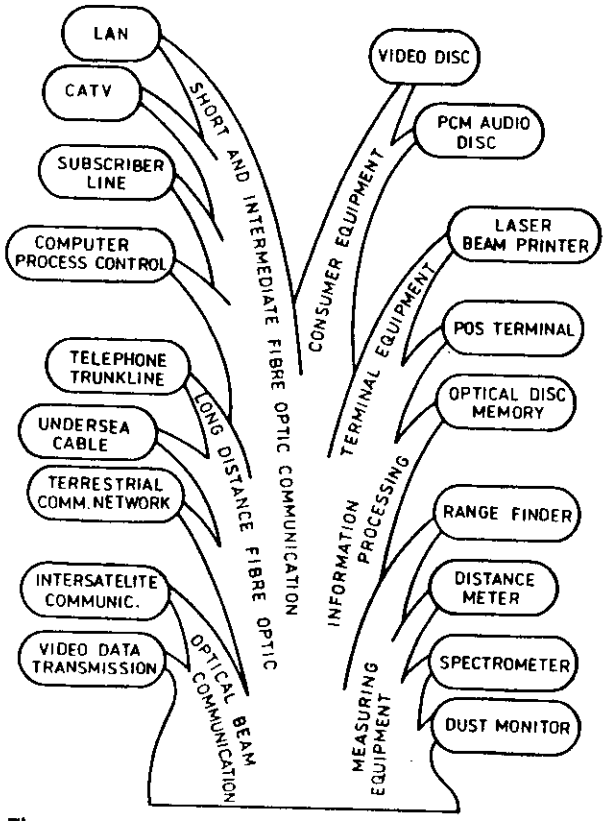

Fig.1.7. The most important technical applications of the optical semiconductor devices range now from optical communications to consumer equipment. Measurement equipment based on semiconductor high power or tunable lasers is emerging

Table 1. Advantages of Fiber Optics

- Large Bandwidth: Light $\sim 10^{14}$ Hz; Modulate >1 GHz
- Low Loss: 1 dB/km; 100 km repeater spacing
- Immune to EM Interference: Dielectric fiber - guided waves
- Complete Electrical Isolation: No common ground
- Lightweight: 2 to 10 x savings
- Rugged and Durable: $\sim 800^{o}C$
- Cheaper: No raw material problems
- Secure: Difficult to tap
- No electrical hazards

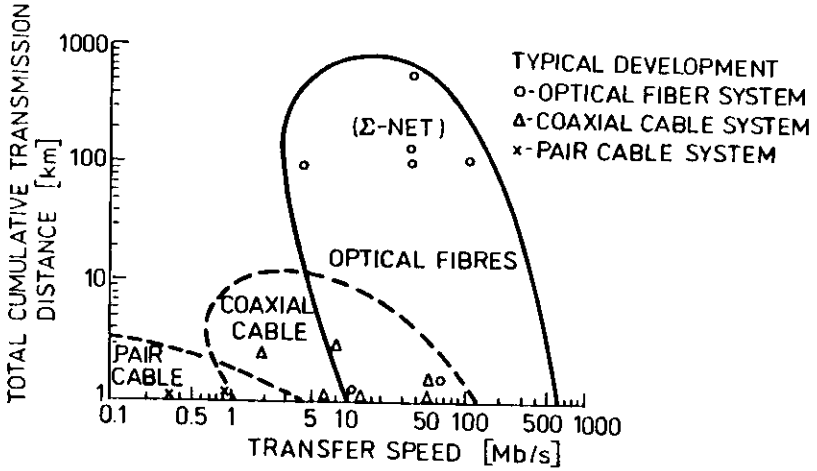

Fig.1.8. Applications of fibre optic Local Area Networks (LAN) optical fibre systems are more suited for high-speed data transfer than pair and coaxial cable systems

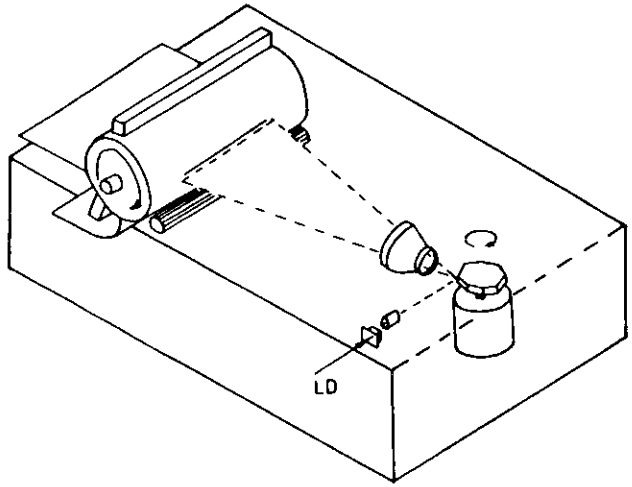

Fig.1.9. Structure of Laser Printer System

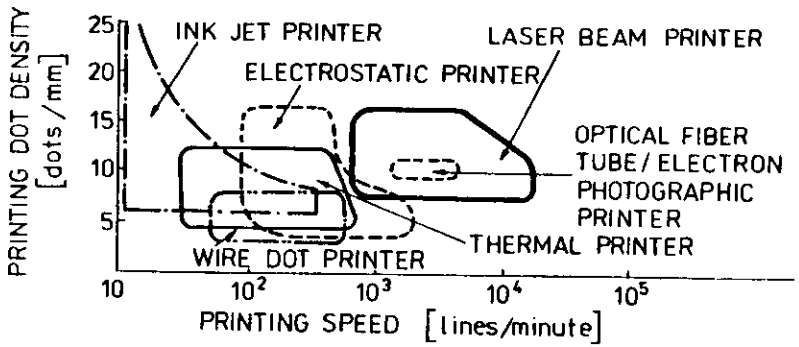

Fig.1.10. Printing speed and dot's density of the "Main Dot-Mode Printer". A laser beam printer can print at high speed with highly resolved images compared with other mode printers. In future, there will be more progress towards higher speed and higher resolution

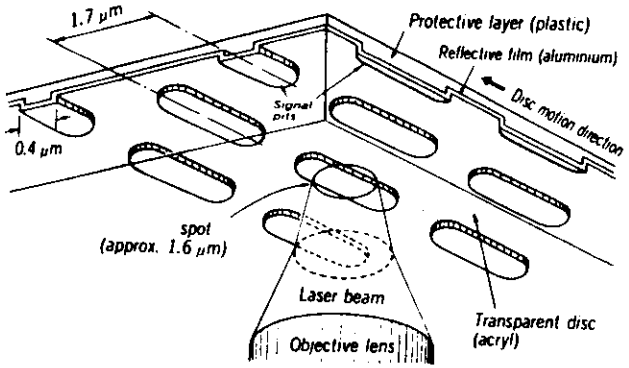

Fig.1.11. Principles of playback of the Optical Video Disc. The laser beam is emitted from under the transparent disc rotating at high speed (1x800)rpm , and the signal is detected from the intensity modulation of the reflected light caused by presence/absence of the signal pit

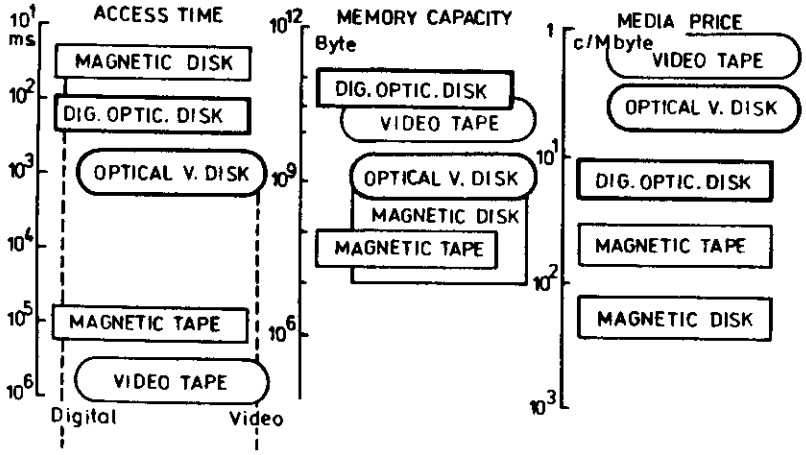

Fig.1.12. Comparison of File Memory Systems. Optical devices coming out enable a short time access video file and/or a large-capacity and low cost digital file systems

2. BASIC DEVICE STRUCTURES AND PARAMETERS

2.1. EMITTERS [1] [2] [3] [4] [5]

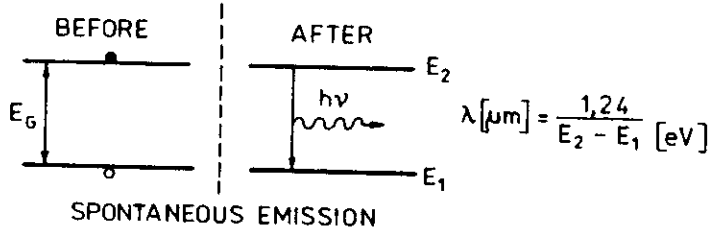

Fig.2.1. Radiative electron-hole recombination leads to spontaneous or stimulating emission. Depending on which of the two processes dominates, the device is called Light Emitting Diode (LED) or LASER

LEDs: Construction Features

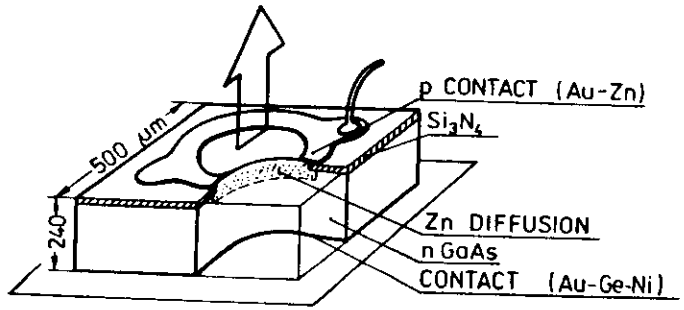

Fig.2.2. Structure of a typical GaAs LED made by selective diffusion of zinc. Similar structures can be obtained using other semiconductor materials eg. $GaAs_xP_{1-x}$

Relevant issues:

- internal quantum efficiency $\eta_i = \dfrac{1}{1 + \dfrac{\tau_r}{\tau_{nr}}}$

- external quantum efficiency $\eta_e = \eta_i \eta_o$

η_o - extraction coefficient

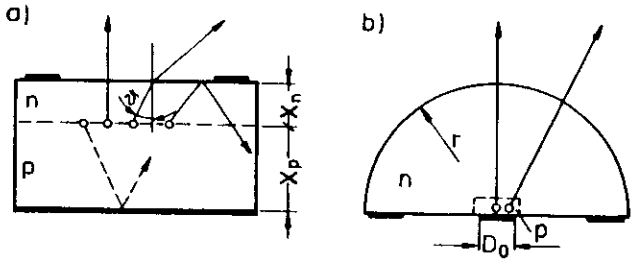

Fig.2.3. Light propagation in two basic LED configurations: a) planar, b) hemisphere

Planar:

$$\eta_o = \frac{[1 + R_c \exp(-2\bar{\alpha}_p x_p)] \exp(-\bar{\alpha}_n x_n)}{n_R (n_R + 1)^2}$$

where: R_c - contact reflectivity, $\bar{\alpha}$ - absorption coefficient, n_R - refraction index, for $n_R = 3{,}6$ and $R_c \approx 0$ $\bar{\alpha} \approx 0$ $\eta_o = 1{,}3\%$

luminance: $L_o = \dfrac{\bar{P}}{\pi n_R (n_R + 1)^2 A_j}$ A_j - emitting area

Hemisphere:

$$\eta'_o = \frac{2 n_R [1 + R_c \exp(-2\bar{\alpha}_p x_p)] \exp(-\bar{\alpha}_n r)}{(n_R + 1)^2}$$

for $n_R = 3{,}6$ $\eta_o \cong 34\%$ $\dfrac{\eta'_o}{\eta_o} \approx 2 n_R^2$

luminance: $L'_o \cong \dfrac{\bar{P}}{\pi n_R (n_R + 1)^2 A_j}$

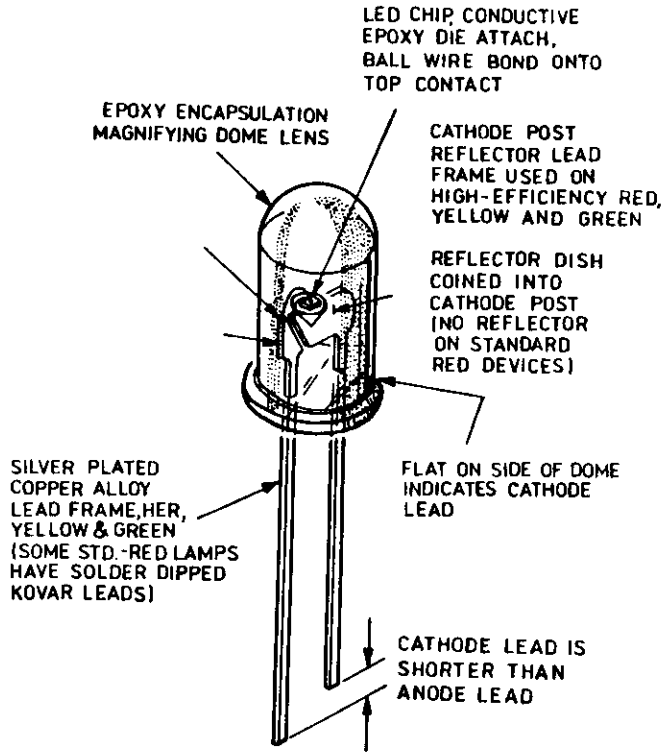

Fig.2.4. Construction features of a plastic encapsulated LED lamp

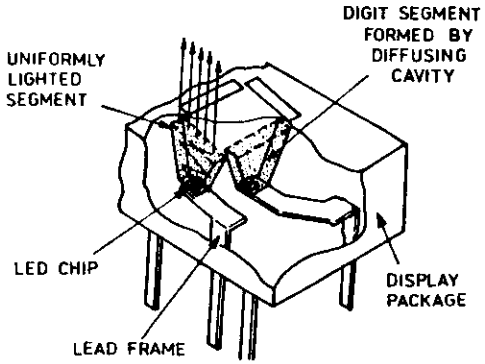

Fig.2.5. Assembly technique of a stretched segment display

LEDs: Materials Considerations and Parameters

visible wavelength range: direct band-gap semiconductors (e.g. $GaAs_xP_{1-x}$ for $x \leqslant 0.49$) or indirect band-gap materials doped with impurities giving iso-electronic trapping (e.g. GaP : ZnO, GaP : N)

infrared range: direct band-gap semiconductors

($Al_xGa_{1-x}As$: $x \leqslant 0.44$)

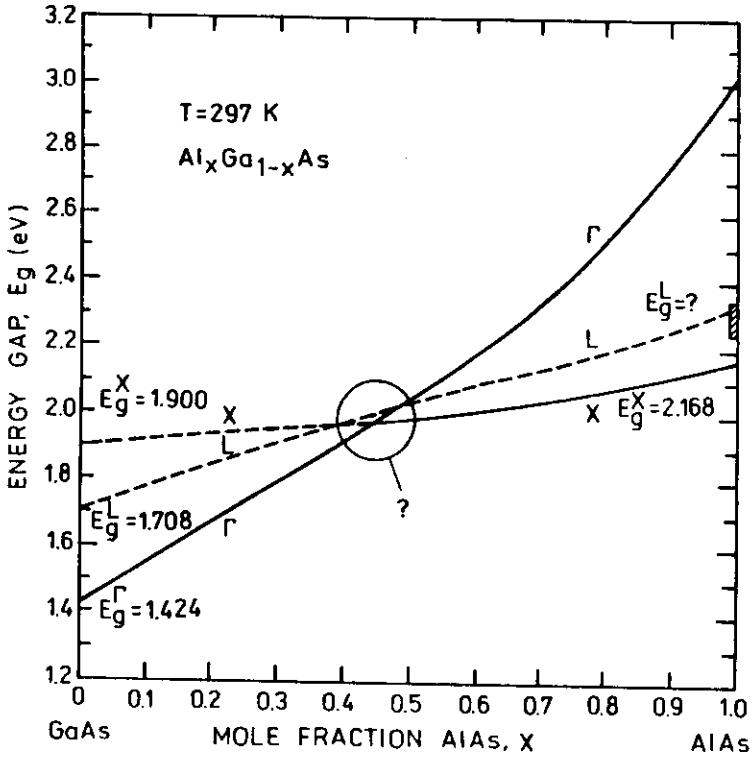

Fig.2.6. Compositional dependence of the energy gap for $Al_xGa_{1-x}As$ [6]

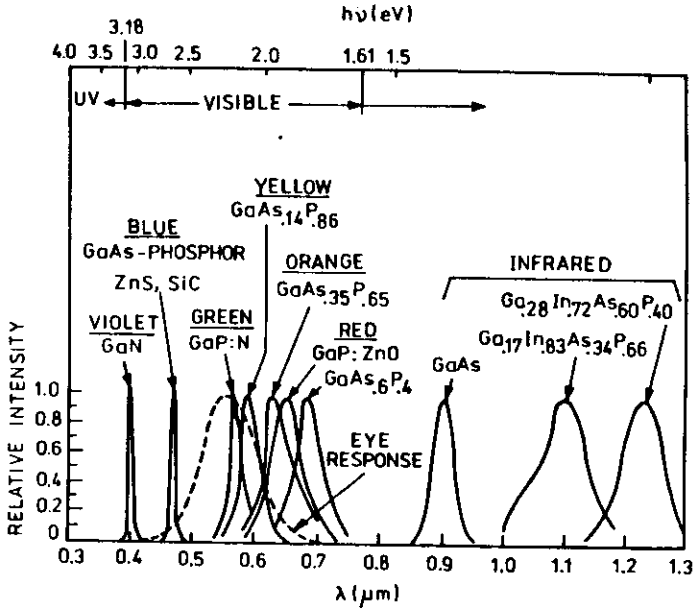

Fig.2.7. Spectral characteristics of typical LEDs

Table 2. Parameters of standard LEDs

Package	Characteristics					
	λ_p [nm]	θ[deg]	P_{out} [mW]	I_F [mA]	t_r [ns]	Material
IREDs TO 18	950	80	8	100	400	GaAs : Si
IREDs TO 18	950	10	8	100	400	Δλ= 50 nm
IREDs Plastic	950	50	10	100	400	
IREDs TO 18	875	30	18	100	500	AlGaAs :Si
	λ_p [nm]	θ[deg]	L[mcd]	I_F [mA]	Δλ [nm]	
VISIBLE LEDs Plastic	660	60	3	20	20	GaAsP/GaAs
	635	65	6	20	45	GaAsP/GaP
	635	24	8	20	45	
	565	24	3	20	35	GaP/GaP
	585	24	10	20	35	GaAsP/GaP

HETEROSTRUCTURES (HETEROJUNCTIONS)

A HETEROJUNTION is a junction in a single crystal between two dissimilar semiconductors. The distinguishing difference is generally the band structure, and the most important feature of the band structure is the energy gap.

Basic configurations

- single heterostructure (SH)
- double heterostructure (DH)
- separate confinement heterostructure (SCH)

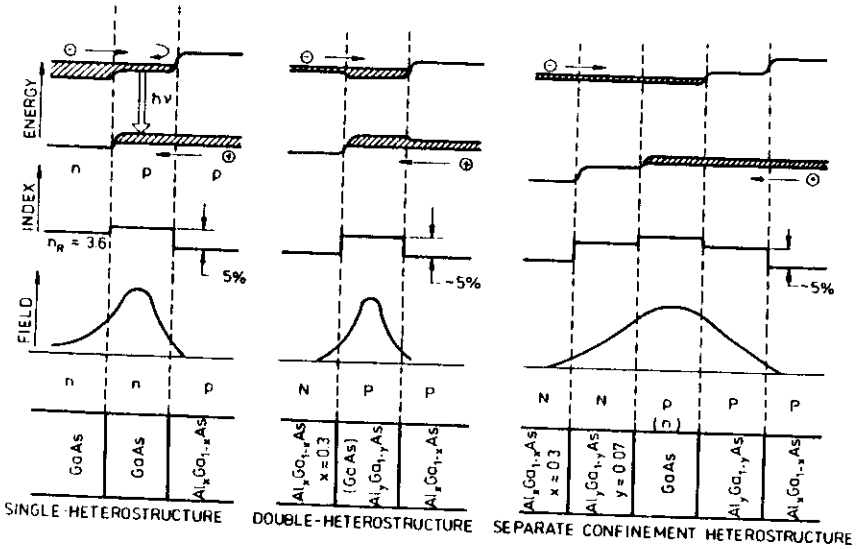

Fig.2.8. Energy band diagram, refractive index profile and optical field distribution in SH, DH and SCH

Advantages: • carrier confinement $\frac{\Delta E}{kT} \geq 8$

• optical field confinement - waveguiding

Materials considerations

- Lattice matching
- wavelength of the emitted radiation

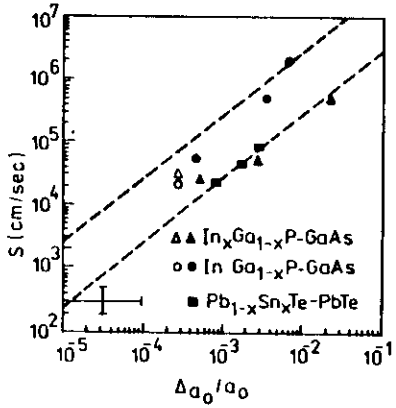

$$\eta_i \cong \frac{1}{1 + \frac{2S}{d}\tau_r}$$

$$S \cong (2 \times 10^7)\frac{\Delta a_o}{a_o}$$

it must be:

$$\frac{\Delta a_o}{a_o} \lesssim 10^{-3}$$

Fig.2.9. Interface recombination velocities for lattice-mismatched heterojunctions as a function of relative mismatch $\Delta a_o/a_o$ [7]

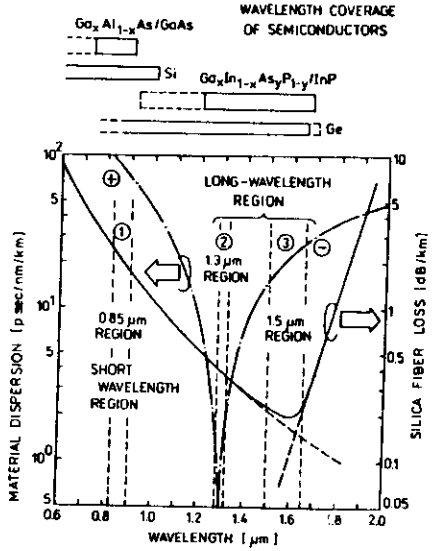

Fig.2.10. Loss spectrum and dispersion versus wavelength of Ge-doped SM fiber. Broken vertical lines indicate wavelength ranges covered by typical semiconductor lasers [8]

Semiconductor Compounds

- Ternary compounds $A^{III}_{B}{}^{V}$
- Quaternary compounds $A^{III}_{B}{}^{V}$

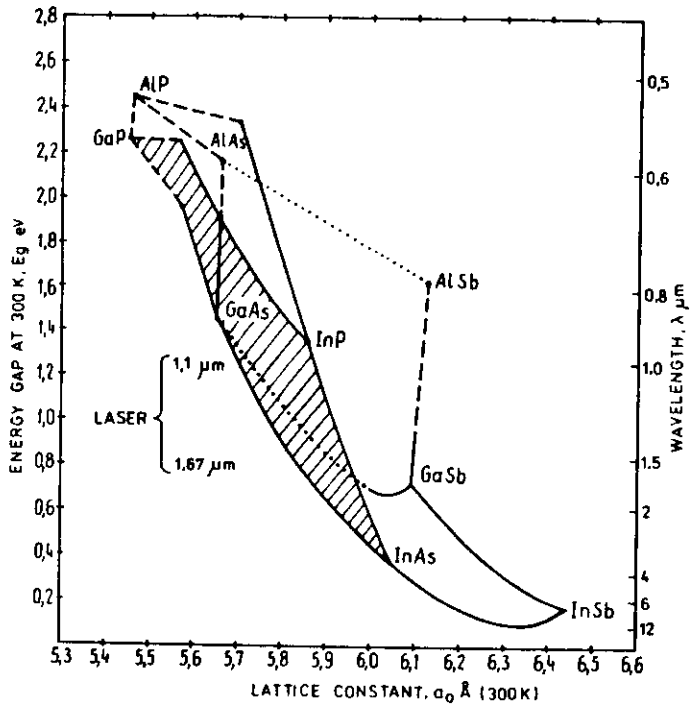

Fig.2.11. Energy gap versus lattice constant of $A^{III}_{B}{}^{V}$ compounds. Note that AlGaAs is lattice matched to GaAs substrates regardless of the composition, other compounds can be lattice matched only if they are quaternaries [4]

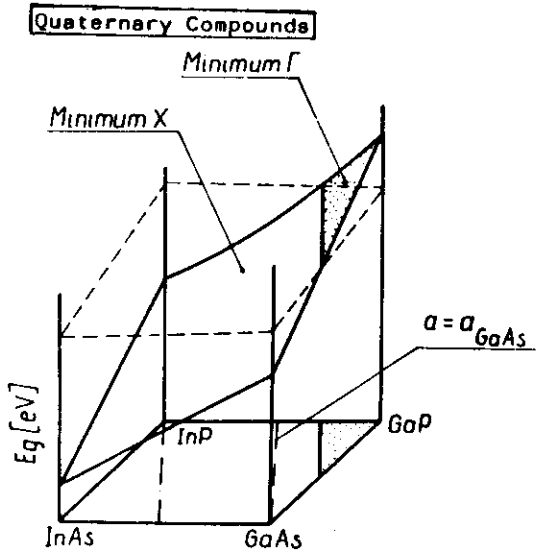

Fig.2.12. Three dimensional diagram showing the relationship between the band-gap and the composition of the quaternary compound InGaAsP

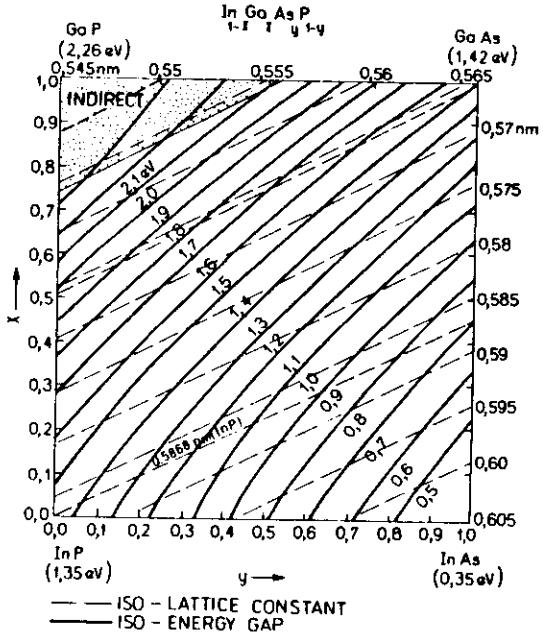

Fig.2.13. Diagram of Fig.2.12 projected on to the base showing the relation-ship between lattice parameter (broken lines) band gap (solid lines) and material composition (x and y axes) for the quaternary material $In_{1-x}Ga_xAs_yP_{1-y}$. Dotted lines indicate compositions lattice matched to InP and GaAs substrates [10]

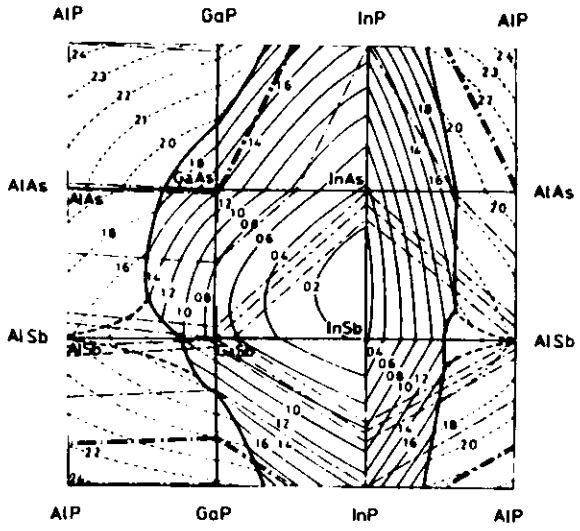

Fig.2.14. Iso-band gap lines versus composition of nine potentially important $A^{III}B^{V}$ compounds. Broken lines denote indirect transitions and cannot be considered for lasers. Typically band gap of the semiconductor used for the active layer of a fibre optic emitter should be within 1,0 - 0,8 eV. Corresponding region has been shadowed on the diagram

Modern concepts of heterostructures

- quantum wells (QW)
- multiquantum wells (MQW)
- strained layer superlattice (SLS)

HETEROSTRUCTURE LEDs

Main application: <u>fibre optic communication systems</u>

<u>Basic structures:</u>

- Surface emitting (SLED) or Burrus type
- Edge emitting (ELED)
- Superluminescent (SLLED)

<u>Important parameters:</u>

- Light - emission center wavelength λ (nm)
- Spectral bandwidth $\Delta\lambda$ (nm)
- Optical output power from fibre end P_F (μW)
- Cutoff frequency or rise time τ(ns), f_c (MHz)
- Forward current I_F (mA)
- Reverse voltage V_R (V)

<u>Relevant issues</u>

- Reliability output power degradation
- Operating temperature

Construction features

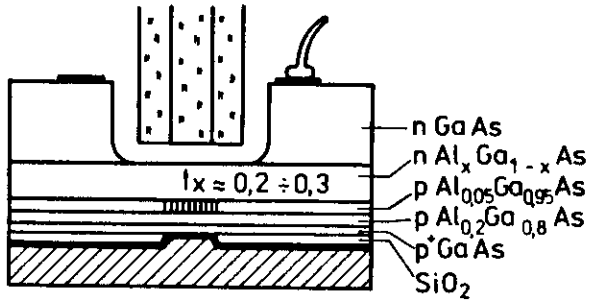

Fig.2.15. Cross-section of a typical Surface Emitting LED, the AlGaAs/GaAs heterostructure passivated selectively by SiO_2 to confine current

Design considerations

- good ohmic contacts
- thermal resistance (must be minimized)
- effective coupling with optical fibre

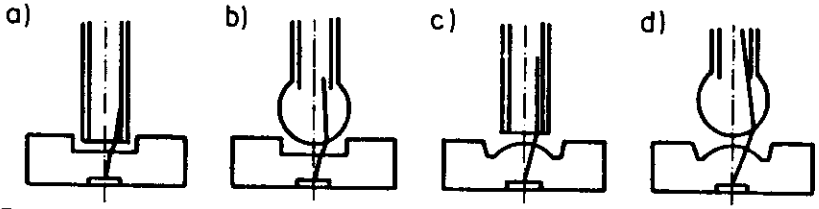

Fig.2.16. Possible configurations of the LED - optical fibre coupling. Results depend on the diameter of the emitting spot, N.A. of the fibre and diameter of its core. For a source smaller than the core and step-index fibre the efficiency $\eta_c \simeq (N.A)^2$

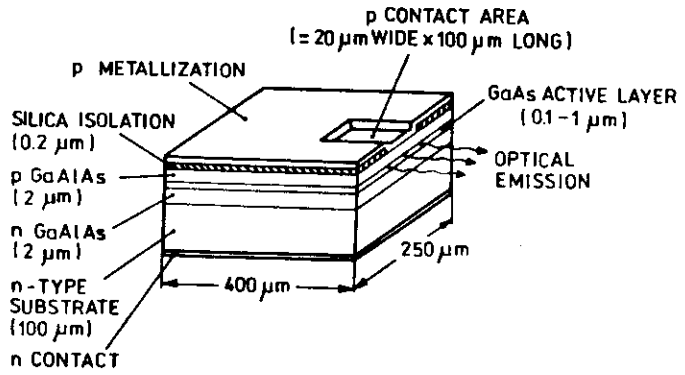

Fig.2.17. Schematic of an Edge - emitting LED. Active region is restricted to a small area in order to increase current density and minimize losses due to absorption

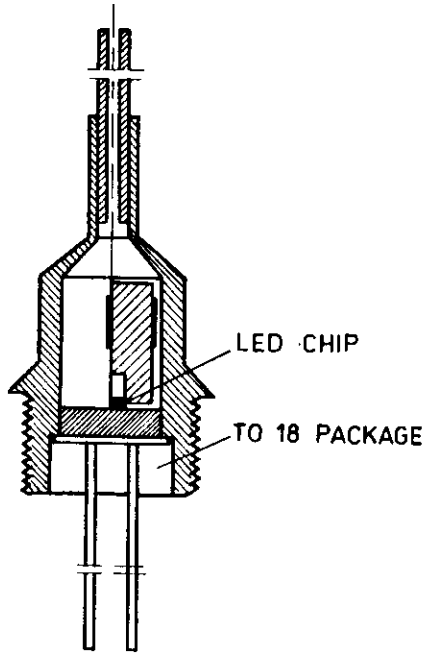

Fig.2.18. Diode package with a short fibre length "pigtail" for easier coupling to fibre cables

Comparison of SLED and ELED

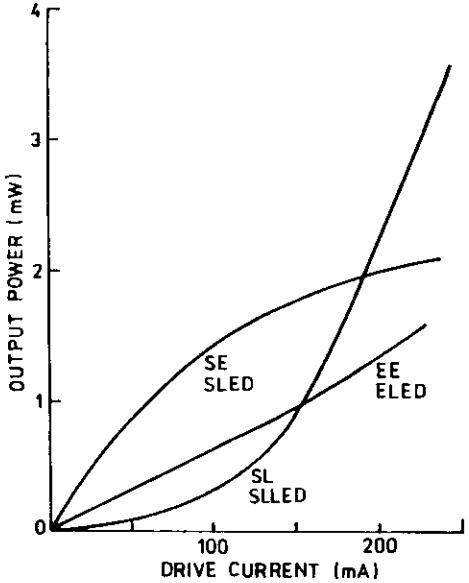

Fig.2.19. Output power versus current for typical surface emitting (SLED), edge emitting (ELED) and superluminescent (SLLED) LEDs

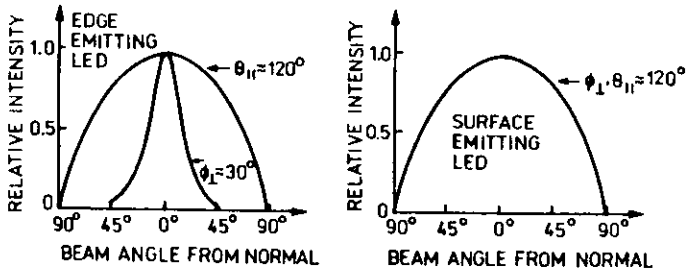

for ELED: $\theta_{\perp} \approx 20 \frac{(\Delta x)d}{\lambda}$ [rad]

Fig.2.20. Far field radiation patterns from an ELED having a very narrow double-heterojunction spacing and a surface emitter

Frequency response

$$P(w) = \frac{P(o)}{\sqrt{1 + (w\tau)^2}} \qquad f_c = \frac{1}{2\pi\tau}$$

where P(o) is the CW output optical power

$$\tau = \frac{ed}{2J}(p_o + n_o)\left\{\left[1 + \frac{4J}{e B_r d (p_o + n_o)^2}\right]^{1/2} - 1\right\}$$

where: p_o and n_o - electron and hole concentrations without injection

d - width of the recombination region

e - electron charge

B_r - recombination coefficient (for GaAs $B_r \simeq 10^{-10}$ cm^3/s at room temp.)

J - current density

at high injection levels:

$$\tau \cong \left(\frac{ed}{B_r J}\right)^{1/2} \qquad f_c = \frac{1}{2\pi}\left(\frac{B_r J}{ed}\right)^{1/2}$$

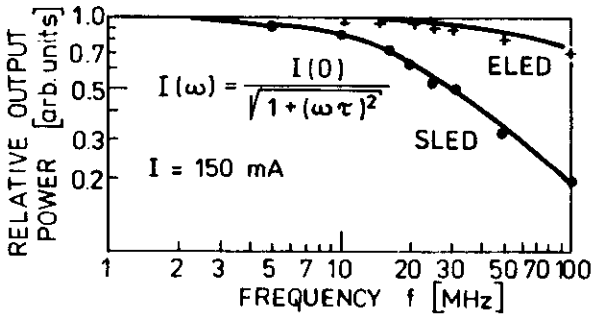

Fig.2.21. Typical frequency response of SLEDs and ELEDs

SEMICONDUCTOR LASERS

Light Amplification by Stimulated Emission of Radiation

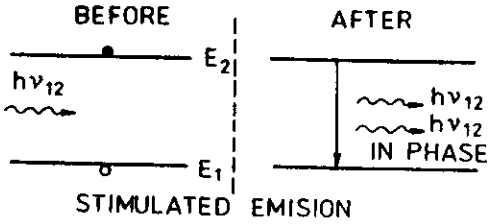

Fig.2.22.

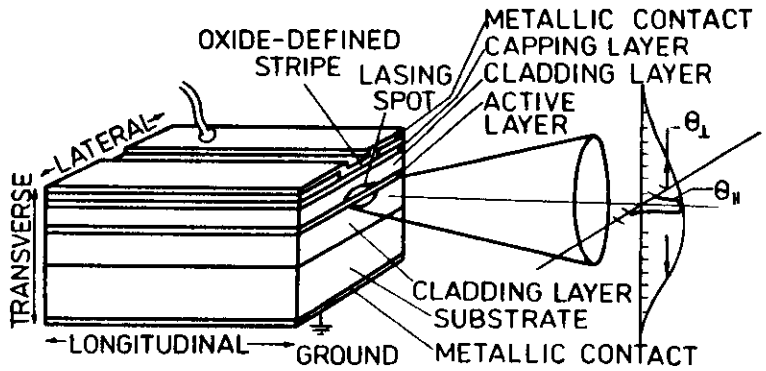

CAPPING LAYER: GaAs (InGaAs)
CLADDING LAYER: AlGaAs (InP)
ACTIVE LAYER: GaAs (InGaAsP)

Fig.2.23. Schematic diagram of a simple heterojunction laser. Stripe-contact double-heterostructure with SiO_2 isolation

Basic Parameters and Characteristics

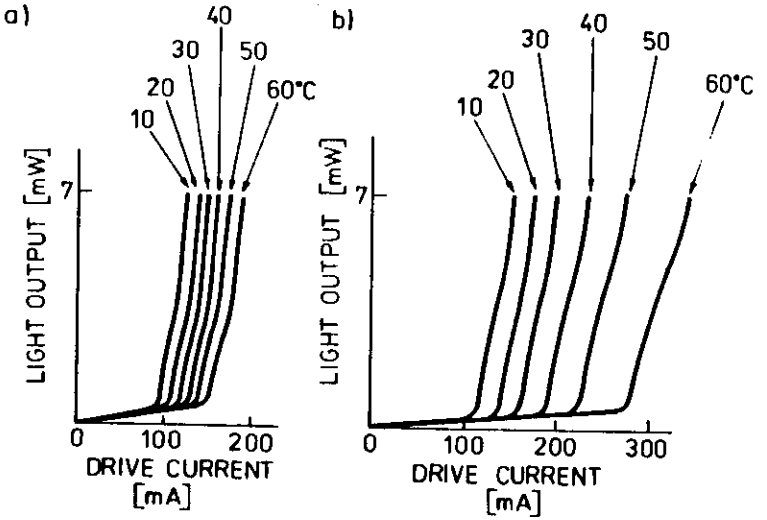

Fig.2.24. Optical output power vs drive current for AlGaAs (a) and InGaAsP (b) lasers as a function of temperature

$$J_{th} = \frac{23d}{\eta_i}\left[\alpha_{out}\left(\frac{1-\Gamma}{\Gamma}\right) + \frac{1}{2L\Gamma}\ln\left(\frac{1}{R_1R_2}\right) + \alpha_{fc} + 180\right]\left[\frac{A}{cm^2}\right]$$

where: d - thickness of the active layer

η_i - internal quantum efficiency

Γ - confinement factor (fraction of the radiation within the recombination region)

R_1, R_2 - reflectivity

α_{out} - absorption coefficient of the material outside the recombination region

α_{fc} - absorption within the recombination region

L - cavity length

$$I_{th} = I_{th}(T_1)\exp\left(\frac{T - T_1}{T_o}\right)$$

T_o - parameter characteristic for the laser structure and material

T_o = 100 - 375K for AlGaAs/GaAs

T_o = 50 - 90K for InGaAsP/InP

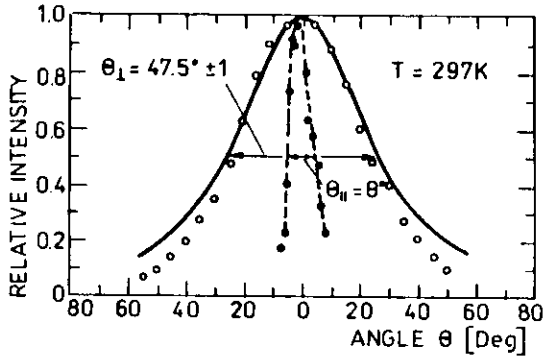

Fig.2.25. Far-field intensity distribution for a DH laser in the direction perpendicular and parallel to the p-n junction plane. Angular width $\theta_\perp$ at the half-power point is a function of d/λ (d - thickness of the active layer) and the index step Δn

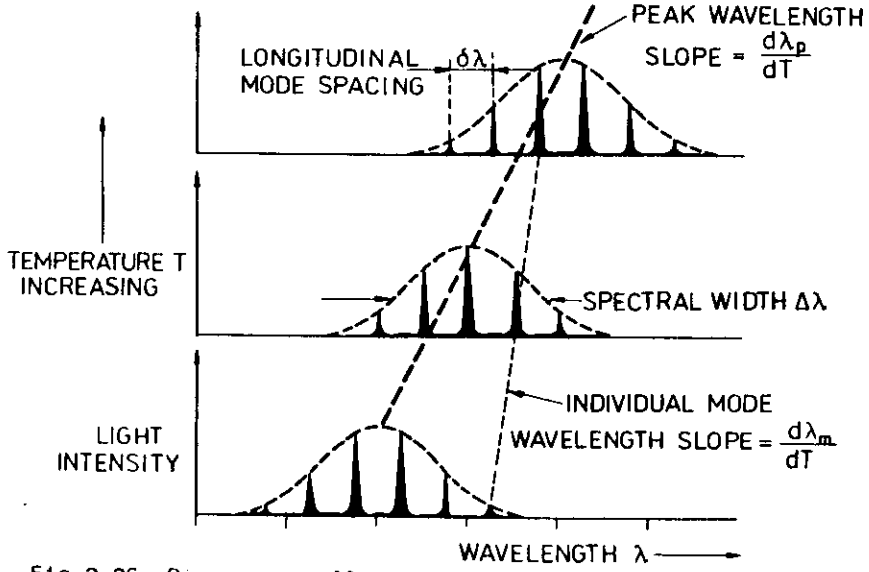

Fig.2.26. Diagram to illustrate emission spectrum of a multimode CW laser and the effect of temperature

SEMICONDUCTOR LASERS: DESIGN CONSIDERATIONS

Transverse Mode and Carrier Confinement

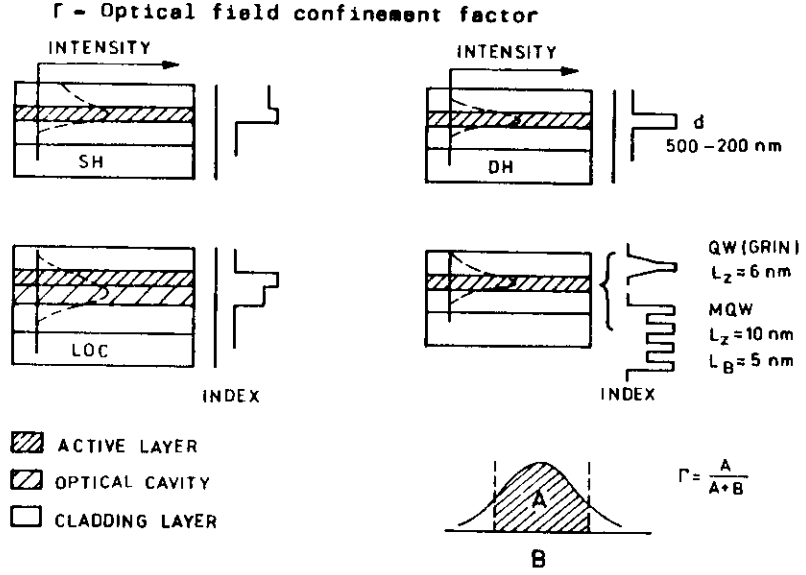

Fig.2.27. Schematic cross section of various laser structures showing geometry and refractive index profile corresponding to variation of the bandgap energy (SH lasers became practically obsolete)

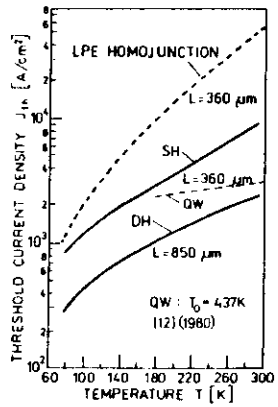

Fig.2.28a. Threshold current density as a function of temperature for various laser structures [11], [12]

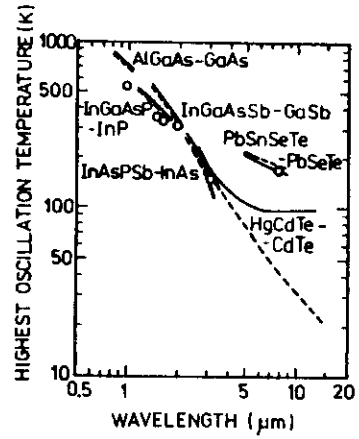

Fig.2.28b. High-temperature limits for laser oscillation in DH lasers under pulsed operation [1]

Lateral Mode Confinement

Stripe lasers: • Gain guided

• Index guided

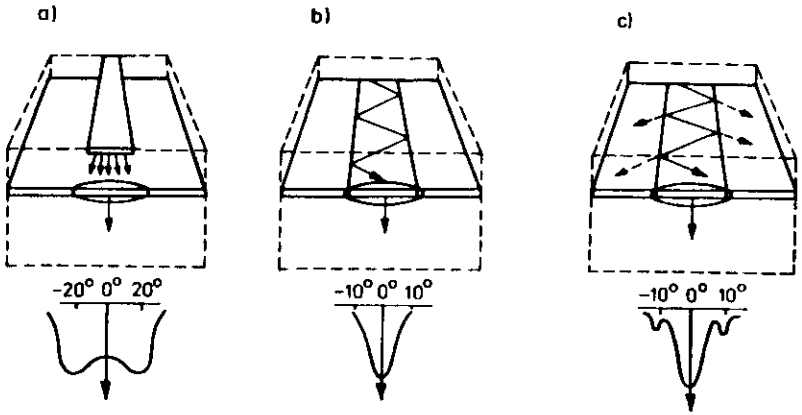

Fig.2.29. Three basic types of wave-confining structures confine the laser light in the lateral direction. In a gain - induced waveguide (left), the injected electrons alter the index of refraction of the active layer, confining the lateral mode; the corresponding beam pattern generally has two peaks and is highly astigmatic. In a positive-index waveguide (center) the central portion of the active region is made to have a higher refractive index than the outer regions; the guided light is totally internally reflected at the dielectric boundaries and provides a Gaussian-shaped beam. In a negative-index waveguide or antiguide (right) the central region of the active layer is made to have a lower refractive index than the outer regions; when light impinges the dielectric boundaries, part of it is reflected back into the waveguide and part of it is refracted into the outer regions. The refracted light is a radiation loss, and it appears in the far field as narrow side lobes

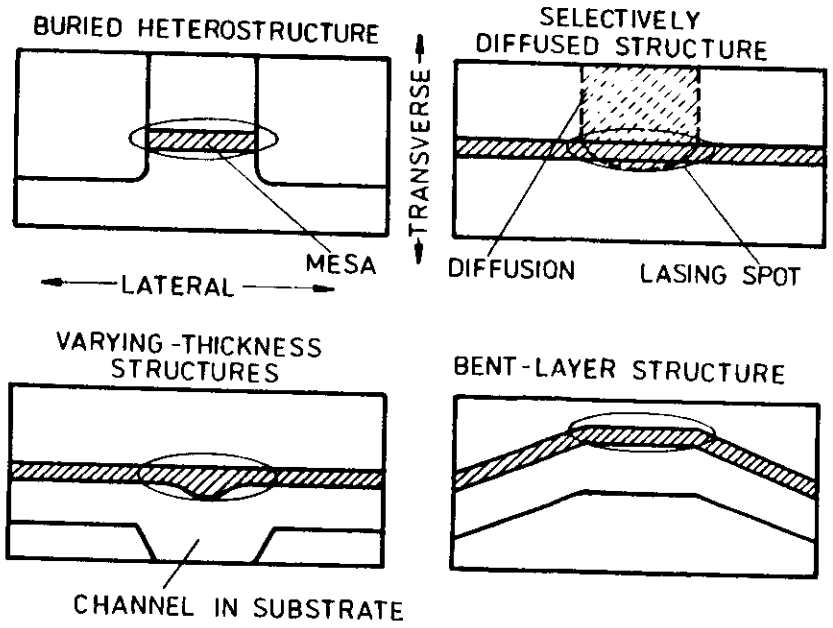

Fig.2.30. Four principal wave-confining structures can be used in index-guided lasers as the waveguides for confining the laser light in the lateral direction. Examples shown are all positive-index waveguides [13]

- buried heterostructure - planar DH material is embeded in a low-refractive index material
- selectively diffused structure - the dopant changes the refractive index of the active layer
- varying-thickness structure - local increase in the thickness forms a positive-index waveguide
- bent-layer structure - lateral bends cause the light "to perceive" a positive-index waveguide, since laterally, light "sees" more low index material outside the bends than in the flat region

Lateral Current Confinement

Necessary for obtaining:
- low threshold current
- high CW output optical power
- high power conversion efficiency

Lateral Current Confinement Schemes

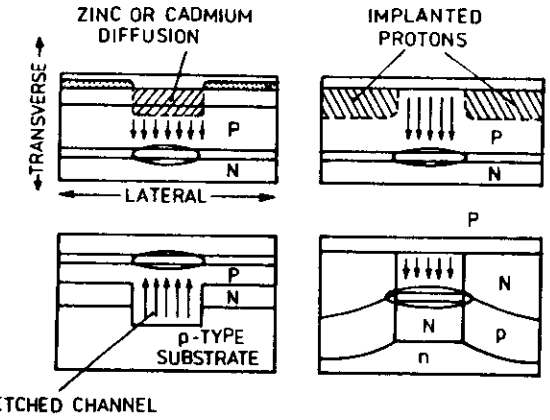

Fig.2.31. Tightly confining the current (arrows) to a narrow strip of the active region is essential for making a CW laser. The four major ways of accomplishing this are shown.

- preferential - dopant diffusion - outside the diffused region the current is blocked by back-biased p-n junctions
- proton implantation - creates regions of high resistivity
- inner stripe confinement - back-biased p-n junctions on both sides of the channel
- buried heterostructure - back-biased p-n junctions

Semiconductor Lasers Designs

There are over 30 ... known laser designs optimized to achieve:
- low threshold current
- single mode operation
- high output power
- special features like small astigmatism of the output beam

Most of those lasers are index guided lasers.

High Power CW Lasers

Main issues:
- facet degradation
- heat generation

Two basic approaches have been taken to avoid facet degradation:

1) Increase the lasing spot size both perpendicular and parallel to the junction and introduce a mode - dependent loss mechanism (lateral antiguiding, lateral absorption, or scattering) to discriminate against high-order-mode oscillation.

2) Eliminate facet degradation by making nonabsorbing mirror (NAM) laser structures.

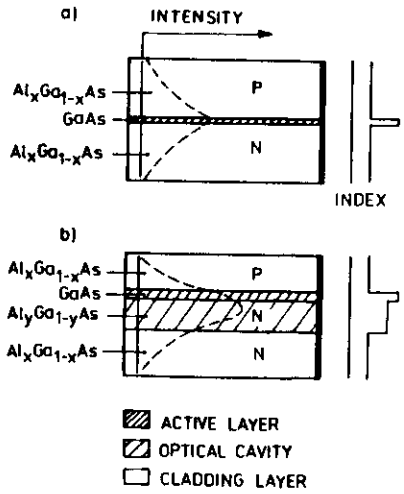

Fig.2.32. One method of increasing the transverse size of the lasing spot is to make a DH diode a very thin active layer (TAL), (left). The TAL acts as a very weak waveguide, so that as much as 90 percent of the optical energy spreads out into the cladding layers. Alternatively, the diode can be constructed with a large optical cavity (LOC) just below the active layer (right). Most of the light propagates in the cavity while obtaining gain from the active layer

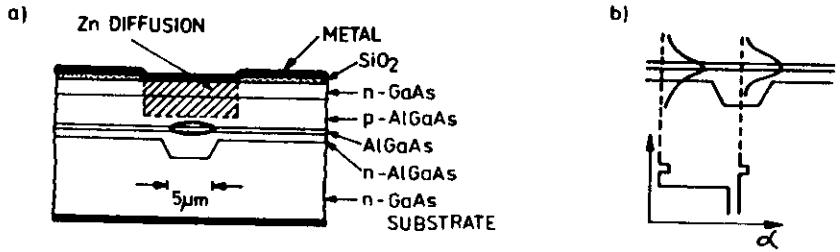

Fig.2.33. Schematic diagram of a CSP (Channeled - Substrate Planar) laser (a) based on the TAL concept [14] and (b): profile of absorption coefficient and resulting variation of the index of refraction

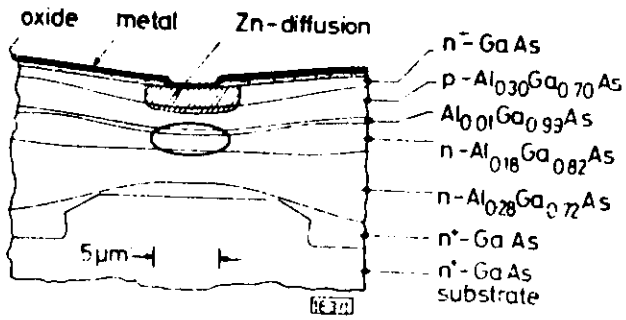

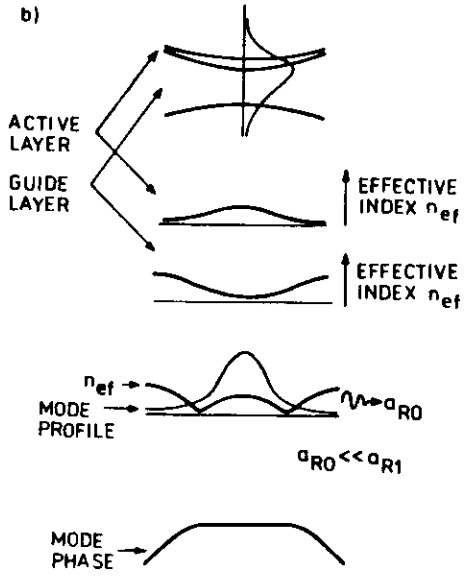

Fig.2.34. Schematic of CHO LOC laser (Constricted Double Heterostructure Large Optical Cavity) (a) and model of the W-shaped lateral "leaky" guide in CDH - LOC structures [15]

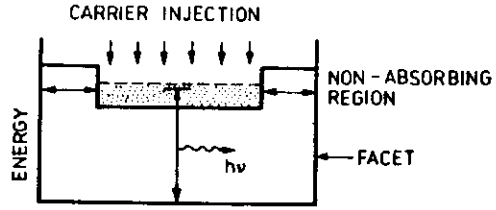

Fig.2.35. Schematic representation of a nonabsorbing mirror (NAM) laser structure

Laser Arrays

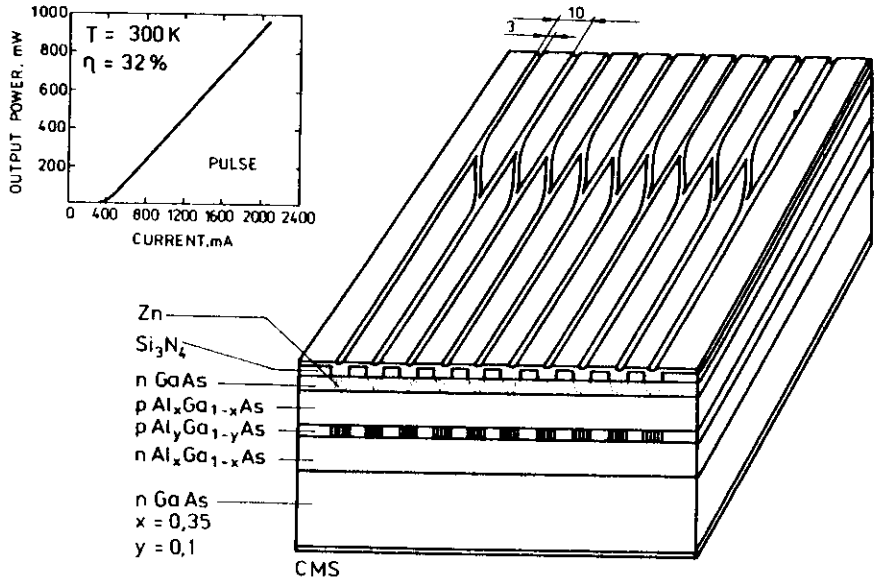

Fig.2.36. Schematic of the coupled multiple stripe (CMS) heterostructure laser. Similar structures have been developed with multiple quantum wells built into the active region [16]

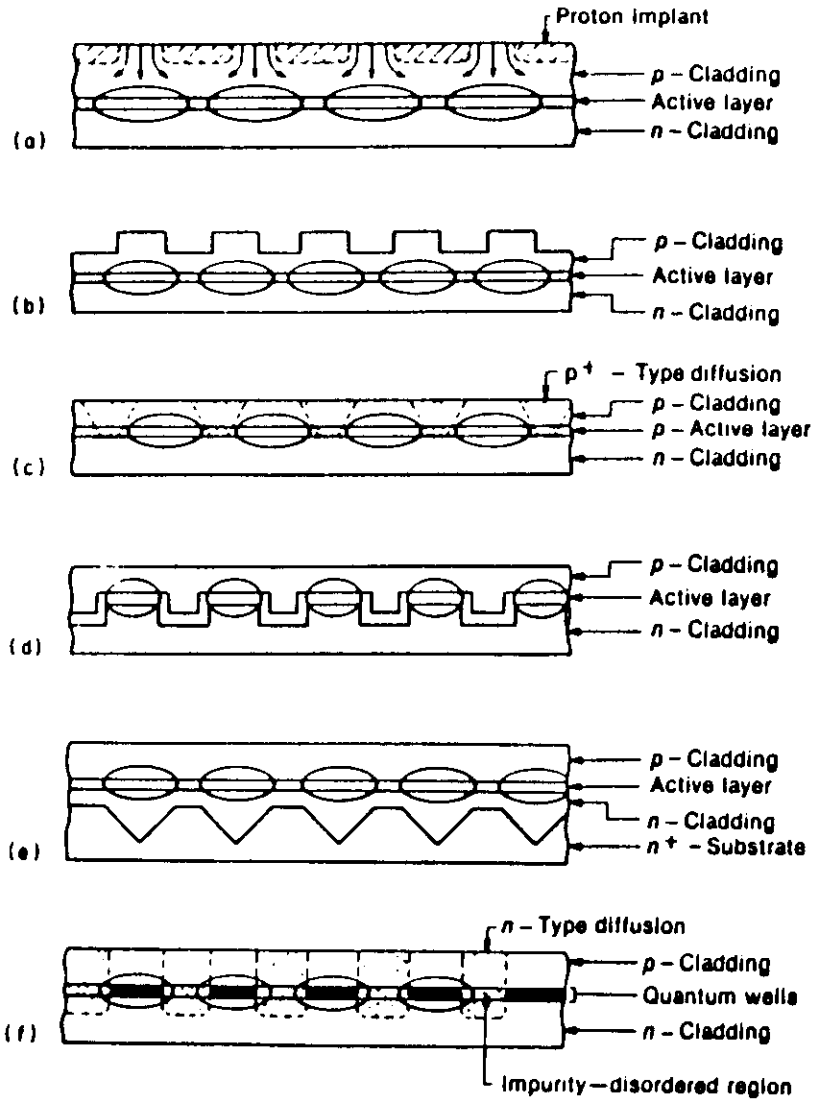

Fig.2.37. Schematic representation of phase locked arrays (see p.44)

Fig.2.37. Schematic representation of phase-locked arrays composed of gain-guided lasers (a), and index-guided lasers [(b) - (f)] fabricated by:
a) preferential proton implantation; b) chemical etching of ridge type waveguides; c) preferential p-type-dopant diffusion; d) metal-organic vapor-phase epitaxial (MOVPE) growth over channeled substrates; e) liquid-phase epitaxial (LPE) growth over channeled substrates; and f) quantum-well-structure disordering induced by preferential n type dopant diffusion. With the exception of the last one, which has been demonstrated only for AlGaAs/GaAs devices, the structure can be either of the AlGaAs/GaAs type or of the InGaAsP/InP type [17]

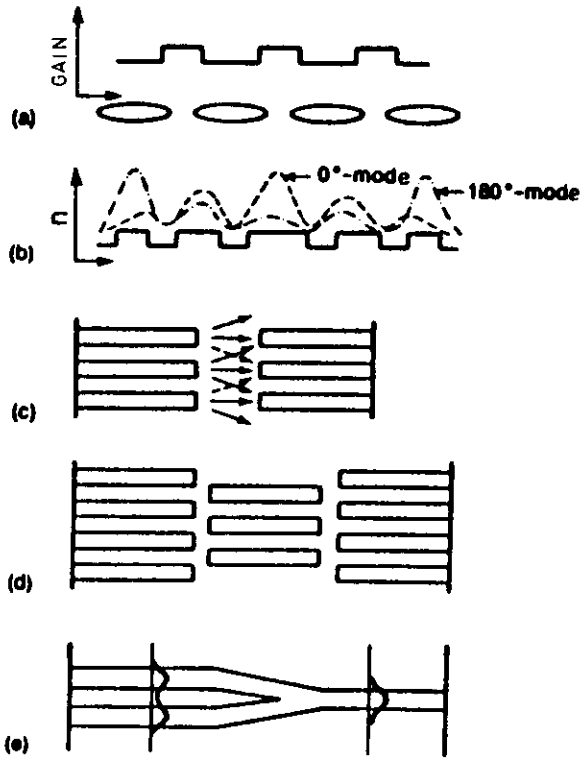

Fig.2.38. The various schemes employed, to date, for achieving fundamental array-mode operation: (a) larger gain between elements than in the elements; (b) "chirped" arrays, (c) diffraction-coupled arrays; (d) offset-stripe arrays; and (e) Y-junction arrays [17]

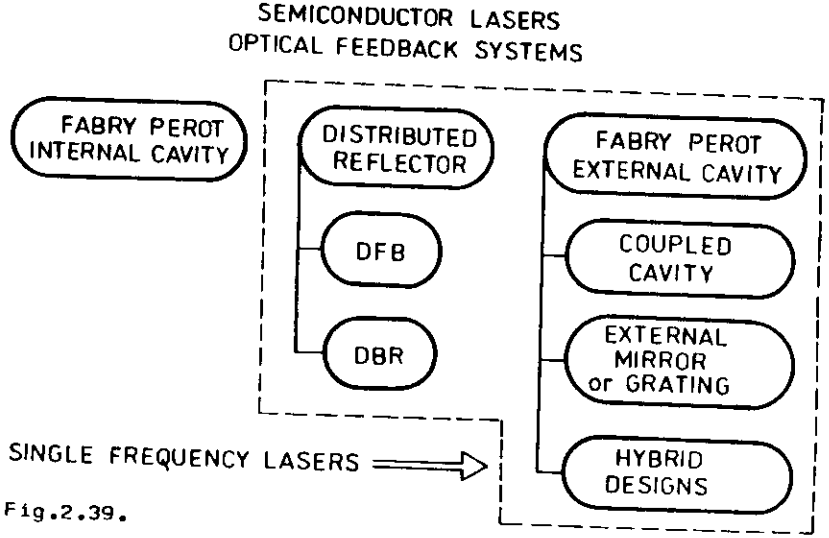

Fig.2.39.

Optical mirrors of Fabry Perot Lasers are obtained by:

- cleaving (along 110 plane)
- cleaving and coating
- etching and cleaving
- etching

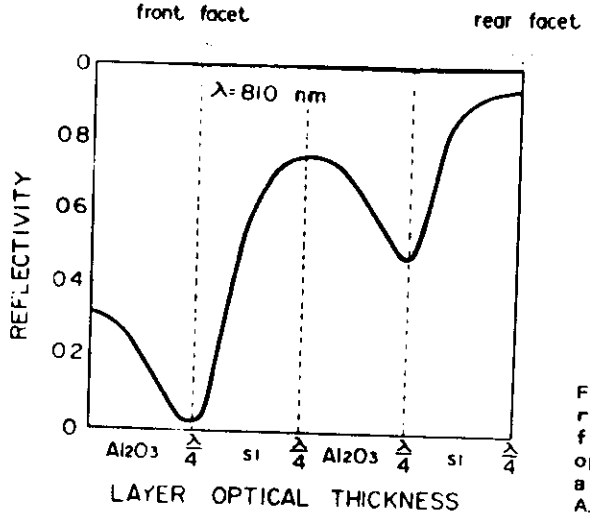

Fig.2.40. Calculated reflectivity as a function of the layer optical thickness for alternating layers of Al_2O_3 and Si [18]

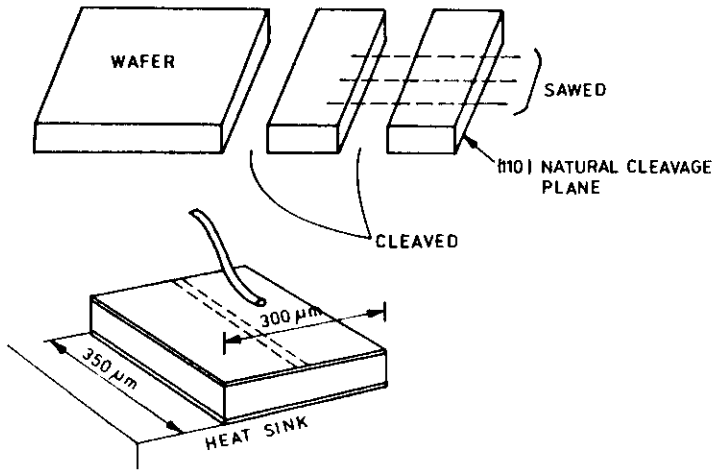

Fig.2.41. GaAs and other III-V compounds can be easily cleaved along (110) crystallographic planes due to specific arrangements of the constituent atoms in the crystal lattice

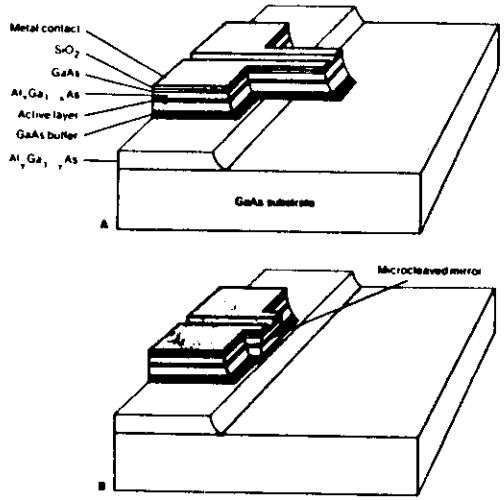

Fig.2.42. When a laser structure about 200 μm long and 20 μm wide is cut by exposure to ultrasonic waves in a liquid bath, a mirror is produced at the laser's base

Distributed Feedback Lasers

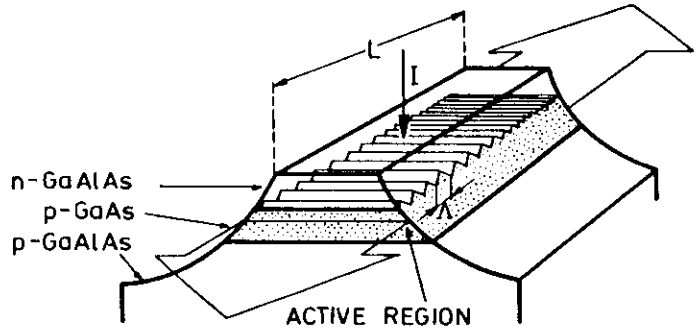

Fig.2.43. Schematic of a DFB laser

Bragg condition: $\Lambda = \frac{\lambda}{2n}$ for $n = 3{,}6$ $\Lambda \cong 1111$ Å

Advantages of the distributed feedback:

- wavelength selection and control (single frequency operation)
- lower sensitivity to temperature changes
- suitable for OEICs (optoelectronic integrated circuits)

Disadvantages of the DFB technology

- two-step epitaxy required
- low output power

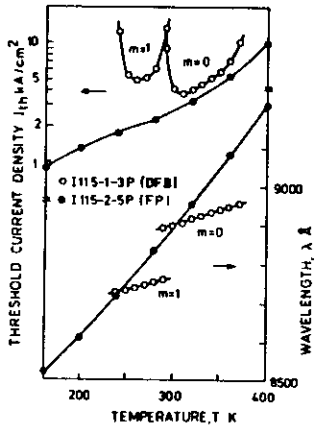

Fig.2.44. Threshold current density and peak wavelength versus temperature characteristics of DFB and FP lasers made of the same heterostructure wafer. DFB lasers are less sensitive to temperature [19]

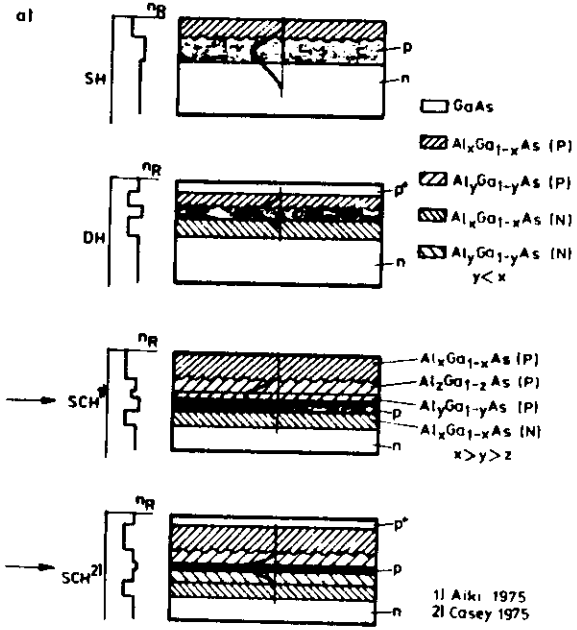

Fig.2.45. Schematics of various possible structures of DFB lasers

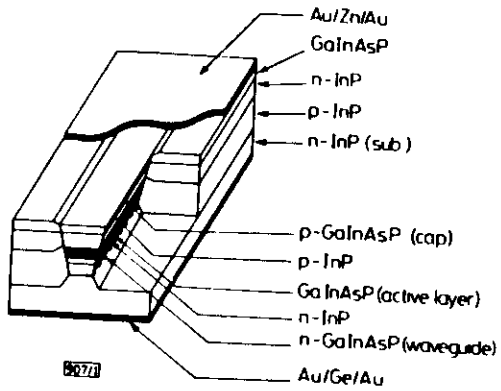

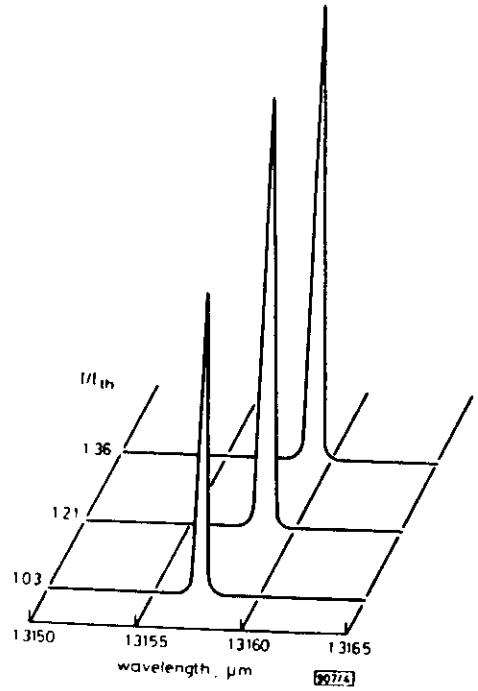

Fig.2.46. An InGaAsP/InP DFB buried heterostructure laser and its spectral characteristics. Fundamental transverse and single longitudinal mode operation has been obtained [20]

Distributed Bragg Reflector Lasers (DBR)

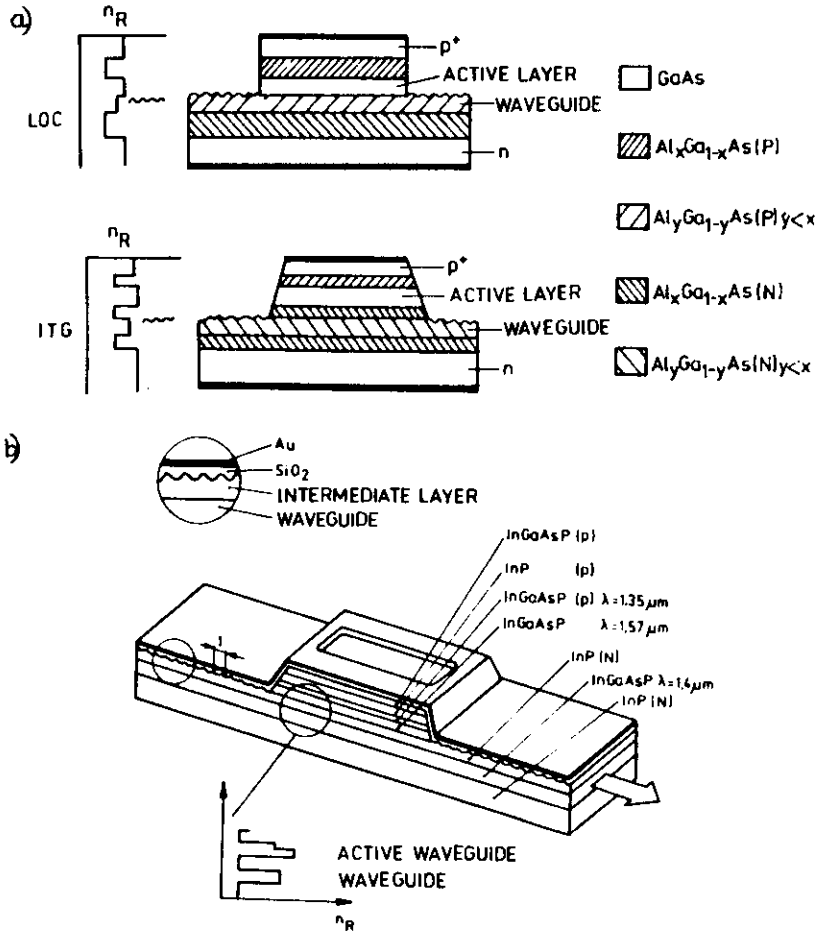

Fig.2.47. Cross-section of DBR laser structures (a) and schematic of an ITG DBR laser (b) [21]

Advantages of the DBR structures:

- more easy to fabricate than DFB
- reflectivity of the distributed mirrors can be independently controlled

Fabry Perot Lasers with External Cavities

The Cleaved-Coupled-Cavity (C^3) laser

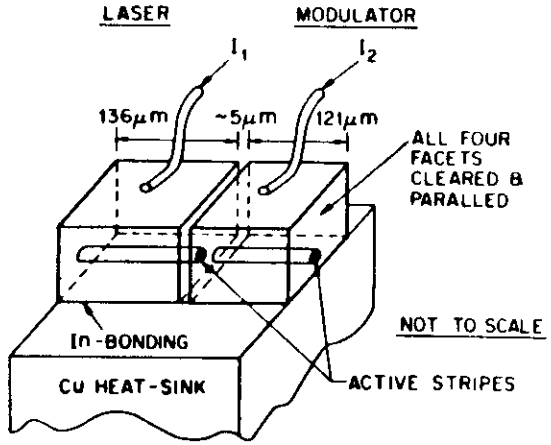

Fig.2.48. Schematic diagram of the C^3 laser [22]

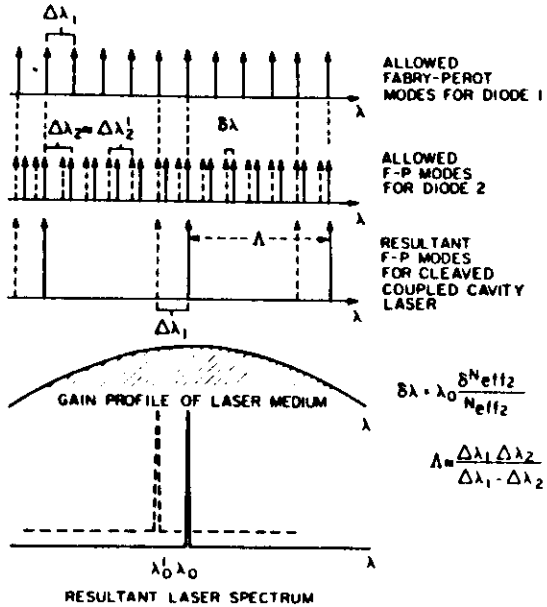

Fig.2.49. Basic working principle of a C^3 laser for obtaing single frequency operation: (a) Allowed Fabry-Perot modes for diode 1, (b) allowed F-P modes for diode 2, (c) resultant modes for double active layer laser, and (d) resultant laser spectrum

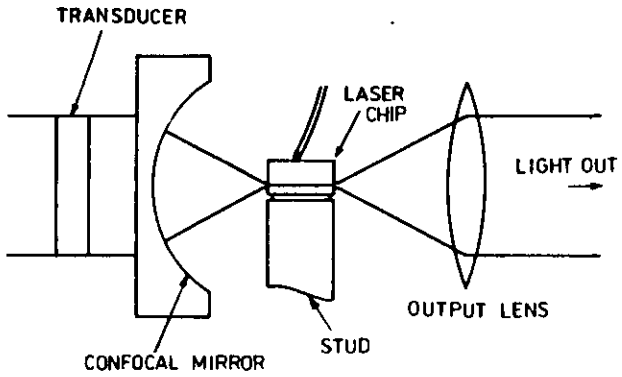

Fig.2.50. Schematic of a heterostructure laser and the confocal external cavity [23]

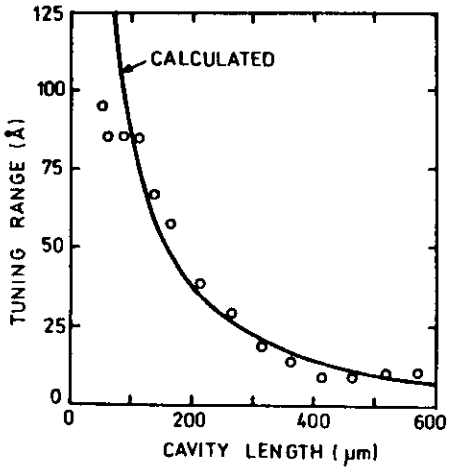

Fig.2.51. The spectral tuning bandwidth as a function of external cavity length obtained using a 240 μm radius mirror [23]

Single Frequency Lasers

(Dynamic Single Mode Lasers - DSM)

Single frequency semiconductor laser: a junction laser that can be made to emit only the fundamental transverse mode and only one longitudinal mode.

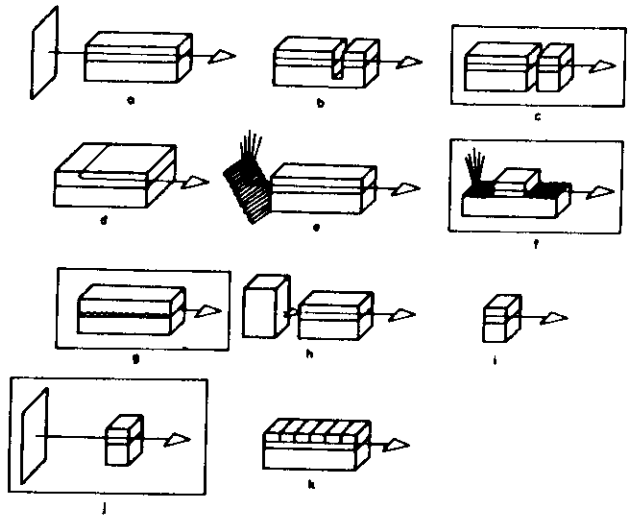

Fig.2.52. There are 11 major designs of single frequency lasers. The three in the top row and the first in the second row are coupled-cavity lasers; the next three are frequency-selective-feedback lasers; the next one is an injection-locked laser; the last one in the third row is a geometry-controlled laser. The two at left are hybrid designs [24]

Table 3. Parameters of selected CW high power single mode lasers [13]

Structure type	Lateral mode discrimination	Max CW power mW	Spot size μm x μm	Lab	Author, year
CDH-LOC+CC	Antiguiding	165	1.4 x 6.0	RCA	Botez et al. 1983
BCM	Scattering	83	1.1 x 2.3	NEC	Endo et al. 1984
CSP	Absorption	95	0.9 x 5.0	Hitachi	Aiki et al. 1978
BTRS	Absorption	200	1.3 x 0.6	Matsushita	Hamoda et al. 1984
DC-PBH+AR	Passive guide	140 (1.3 μm)	1.1 x 2.5	NEC	Mito et al. 1985
PBC	Passive guide	85 (1.3 μm)	0.9 x 2.2	Mitsubishi	Sakakibara et al. 1985

Tunable Infrared Semiconductor Lasers

Application: Infrared spectroscopy

Required features: • tunability

• extremely narrow emission line-width

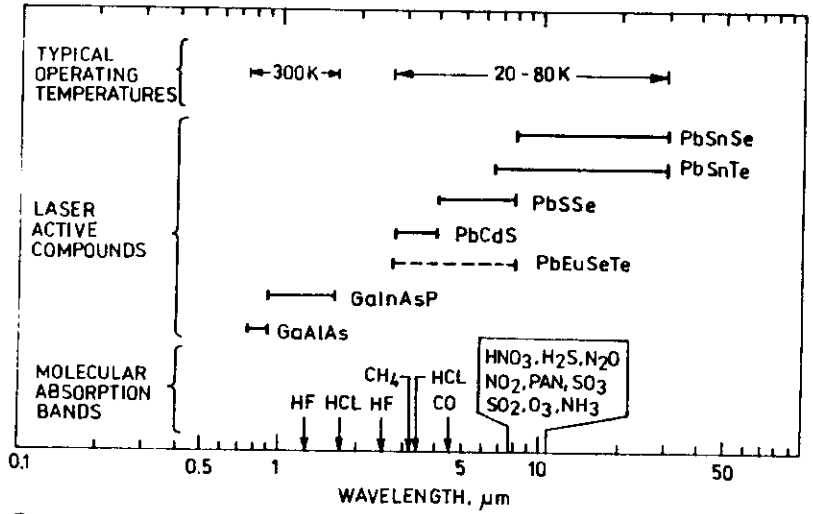

Fig.2.53. Properties of heterojunction lasers relevant to spectroscopy applications [25]

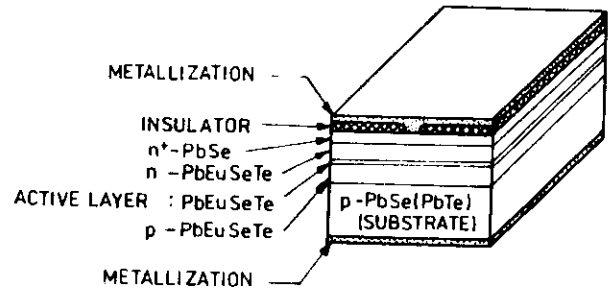

Fig.2.54. Double heterostructure lead salt laser configuration (Maximum operating temperature: CW - 150K, pulse - 250K) Note: these new types of lasers are still in the laboratory state [25]

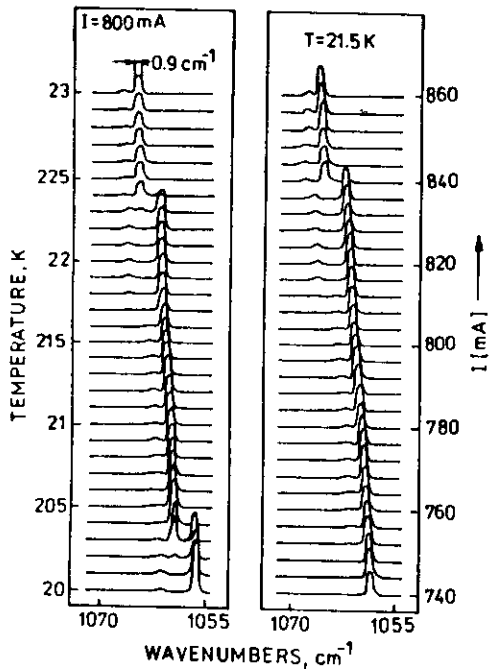

Fig.2.55. Temperature and current tuning characteristics of a $Pb_{0,995}Sn_{0,005}Se$ heterojunction laser [25]. Since gas absorption lines exhibit linewidths of a few 0.1 cm^{-1} at normal pressure and in the order of 0.01 cm^{-1} at reduced pressure, the emitted laser radiation can be easily tuned through a selected gas absorption line with a resolution of $< 10^{-4} cm^{-1}$ far below the linewidth

2.2. PHOTODETECTORS [26], [27]

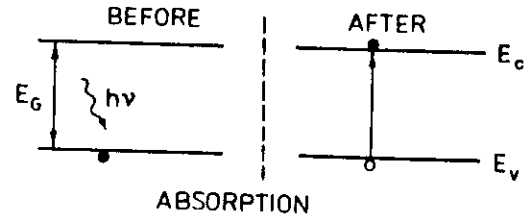

Fig.2.56. Photon absorption resulting in freecarrier generation is fundamental for operation of semiconductor photodetectors

The major requirements for a photodetector and optical receiver with high performance include:

- large response at the wavelength of the incident optical signal
- sufficient electrical bandwidth i.e. speed of response, to accomodate the information bandwidth of the incoming signal
- minimum excess noise introduced by the detection and amplification process.

GENERAL INFORMATION

Figures of Merit

Figures of merit are used to compare the measured performance of one photodetector against the measured performance of other photodetectors of the same class, the performance expected of an ideal photodetector that performs at a level limited by some fundamental physical principle. Care in the use of photodetector figures of merit is essential because many parameters of photodetector performance do not fully summarize the relevant factors in photodetector choice.

A basic figure of merit that applies to all detectors with electrical output is responsivity.

• Responsivity

Responsivity is the ratio of the output (usually in amperes or volts) to the radiant input in(watts).

Spectral voltage responsivity:

$$R_v(\lambda, f) = \frac{V_s}{P_{opt}(\lambda)} \quad [V/W]$$

V_s - measured voltage output

P_{opt} - spectral radiant power incident on the detector

Alternatively:

$$R_i(\lambda, f) = \frac{I_s}{P_{opt}(\lambda)} \quad [A/W]$$

It may be noticed that

$$R_i = \frac{\eta q}{h\nu} = \frac{\eta \lambda}{1.24} \quad [A/W]$$

where: λ in μm

η - quantum efficiency

The blackbody responsivity:

$$R_v(T, f) = \frac{V_s}{\int_0^\infty P_{opt}(\lambda)\, d\lambda} = \frac{V_s}{A_s \sigma \varepsilon T^4 A_d / \pi R^2}$$

is equal to the ratio of detector output and incident radiant power from a blackbody source of temperature T modulated at a frequency f that produces the observed output.

• Quantum Efficiency η

The Quantum efficiency η is the number of electron-hole pairs generated per incident photon

$$\eta = \frac{I_s}{q} \frac{P_{opt}}{h\nu}$$

where: I_s is the photogenerated current by the absorption of incident radiant power P_{opt} at a wavelength λ

• Noise Equivalent Power (NEP)

The Noise Equivalent Power of a detector is the required power incident on the detector to produce a signal output equal to the rms noise output.

$$NEP = \frac{i_{rms}}{R_i}$$

where: i_{rms} is the root-mean-square noise current in amperes, R_i is the current responsivity in A/W.

Detectivity D

The detectivity D of a detector is the reciprocal of the noise equivalent power.

$$D = \frac{1}{NEP}$$

• Normalized Detectivity D^*

The normalized detectivity D^* normalizes the detector area and bandwidth

$$D^* = D\sqrt{A_d \Delta f} = \frac{\sqrt{A_d \Delta f}}{NEP} \quad [cm\ Hz^{1/2}\ W^{-1}]$$

Alternatively

$$D^* = \frac{\sqrt{A_d \Delta f}}{V_{rms}} \times R_v = \frac{\sqrt{A_d \Delta f}}{i_{rms}} \times R_i = \frac{\sqrt{A_d \Delta f}}{P_{opt}} \left(\frac{S}{N}\right)$$

where $\frac{S}{N}$ is the signal to noise ratio.

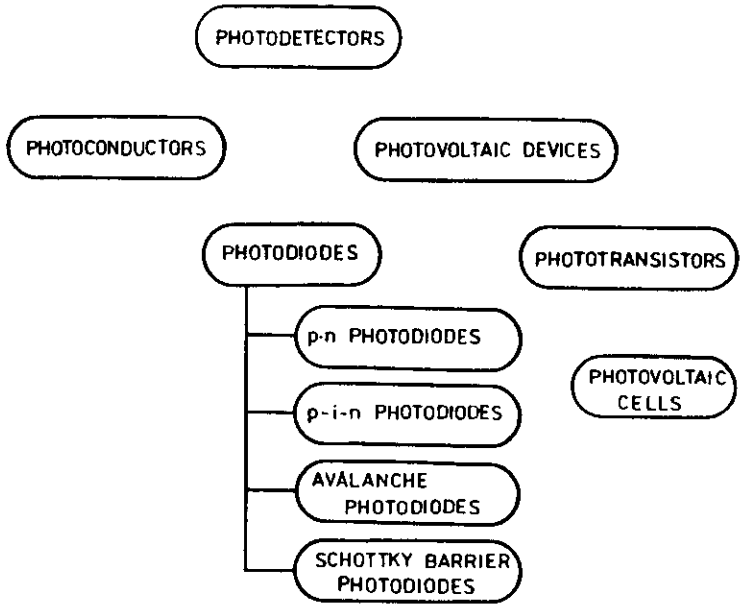

Fig.2.57. General classification of major types of semiconductor photodetectors

PHOTOCONDUCTORS

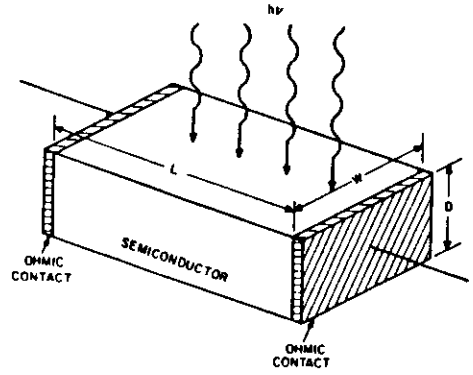

$$I_p = q(\eta \frac{P_{opt}}{h\nu})(\frac{\mu_n \tau \mathcal{E}}{L})$$

$I_{ph} = q(\eta \frac{P_{opt}}{h\nu})$ primary photocurrent

$$\text{gain} = \frac{I_p}{I_{ph}} = \frac{\mu_n \tau \mathcal{E}}{L} = \frac{\tau}{t_r}$$

$$t_r = \frac{L}{V_d}$$

Fig.2.58a) Schematic diagram of a photoconductor that consists of a slab of semiconductor and two ohmic contacts at the ends

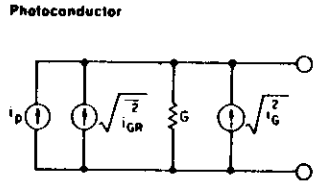

Fig.2.58b) Equivalent circuit of a photoconductor

the rms signal current:

$$i_p \approx \frac{q\eta m P_{opt}}{\sqrt{2}\, h\nu} \left(\frac{\tau}{t_r}\right) \frac{1}{(1 + \omega^2\tau^2)^{1/2}}$$

thermal noise:

$$i_G^2 = 4\, kT\, G\, B$$

shot noise:

$$i_{GR}^{-2} = \frac{\tau}{t_r} \frac{4\, q\, I_o\, B}{1 + \omega^2\tau^2}$$

$$(S/N)_{power} = \frac{i_p^2}{\overline{i_{GR}^{\cdot 2}} + \overline{i_G^{\cdot 2}}} = \frac{\eta m^2 (P_{opt}/h\nu)}{8\, B} \left[1 + \frac{kT}{q} \frac{t_r}{\tau}(1 + \omega^2\tau^2) \frac{G}{I_o}\right]^{-1}$$

PHOTODIODES

p-n and p-i-n Photodiodes

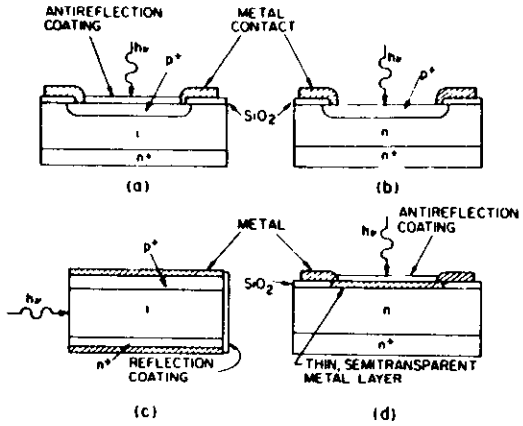

Fig.2.59. Device configurations of some high-speed photodiodes [28]:
a) p-i-n diode,
b) p-n diode,
c) p-i-n diode with illumination parallel to junction,
d) metal-semiconductor (Schottky barrier) diode

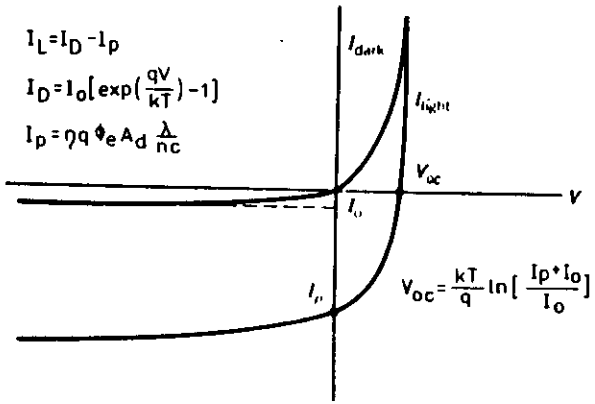

Fig.2.60. p-n junction current-voltage characteristic and its shift during exposure to light. I_p is the photocurrent, Φ_e is the incident radiant flux density

Noise Properties

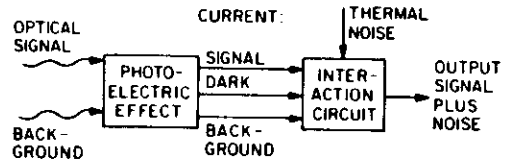

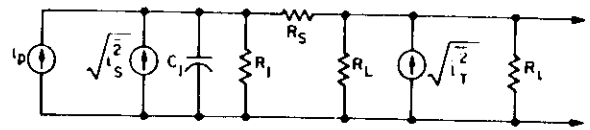

Fig.2.61a) Photodetection process of a photodiode. b) Equivalent circuit of a photodiode [26]

rms signal current:

$$i_p = q\eta \, P_{opt}/\sqrt{2}\, h\nu$$

shot noise

$$\langle i_s^2 \rangle = 2\, q\, (I_p + I_B + I_D)\, B$$

I_p - photocurrent,
I_B - current resulting from background radiation
I_D - dark current
B - bandwidth

thermal noise

$$\langle i_T^2 \rangle = 4\, kT\, (1/Req)\, B \qquad R_{eq} = 1/R_j + 1/R_L + I/R_i$$

$$(S/N)_{power} = \frac{i_p^2 R_{eq}}{(\langle i_s^2 \rangle + \langle i_T^2 \rangle) R_{eq}} = \frac{1/2 (q\eta P_{opt}/h\nu)^2}{2\, q\, (I_p + I_B + I_D) B + 4kTB/R_{eq}}$$

Metal-Semiconductor (Schottky Barrier) Photodiodes

Metal-semiconductor photodiodes are particularly useful in the visible and ultraviolet regions. In these regions the absorption coefficients α in most of the common semiconductors are very high, of the order of 10^5 cm^{-1} or more, corresponding to an effective absorption length of $1/\alpha \cong 0.1$ μm or less. It is possible to choose a proper metal & a proper antireflection coating so that a large fraction of the incident radiation will be absorbed near the surface of the semiconductor.

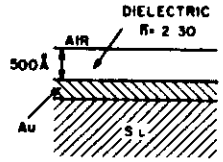

(a)

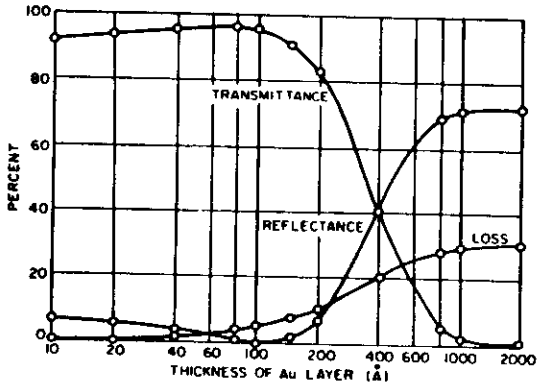

(b)

Fig.2.62. (a) A 500 Å - thick ZnS antireflection coating. (b) Transmittance, reflectance, and loss in the gold films as a function of the gold layer thickness, $\lambda = 0.6328$ μm [29]

Avalanche Photodiodes

Relevant issues:
- low noise
- high gain
- high speed
- reasonably high operation voltage

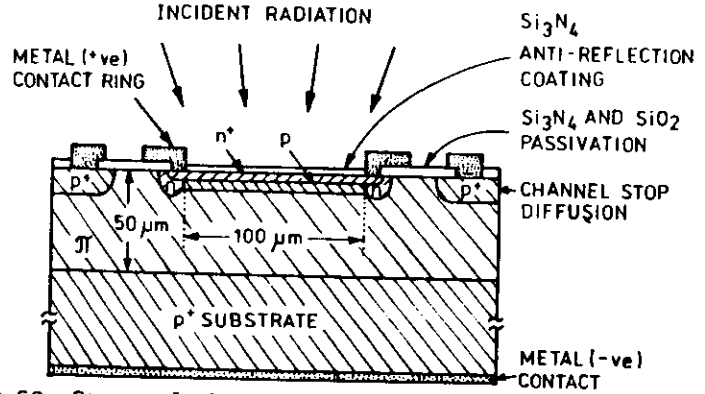

Fig.2.63. State-of-the-art reach through silicon avalanche photodiode structure [30]. Guard rings are made to prevent premature breakdown, channel stop rings are to prevent surface leakage

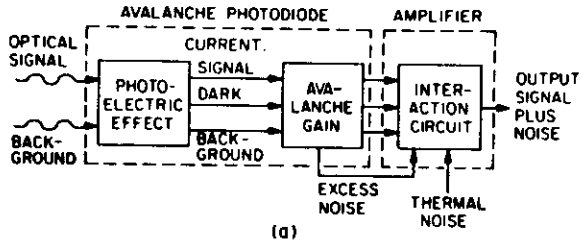

(a)

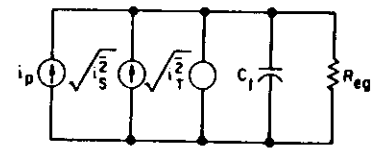

(b)

Fig.2.64a) Photodetection process, b) Equivalent circuit for APD [26]

Noise Properties of APD

$i_p = q\,\eta\,m\,\phi_e\,M\sqrt{2}\,h\nu$ M - avalanche gain

$\langle i_s^2 \rangle = 2q\,(I_p + I_B + I_D)\langle M^2 \rangle B$

or

$\langle i_s^2 \rangle = 2q\,(I_p + I_B + I_D)\,M^2\,F(M)B$

$$S/N = \frac{1/2\,(q\eta P_{opt}/h\nu)^2}{2q\,(I_p + I_B + I_D)\,F(M)B + 4\,kT\,B/R_{eq}\,M^2}$$

Noise Factor:

$$F(M) = \langle M^2 \rangle / M^2$$

for electron injection alone:

$$F(M) = \beta/\alpha\,M + (2 - 1/M)\,(1 - \beta/\alpha)$$

α - electron ionization rate
β - hole ionization rate

small β/α is required for electron injection and
small α/β for hole injection

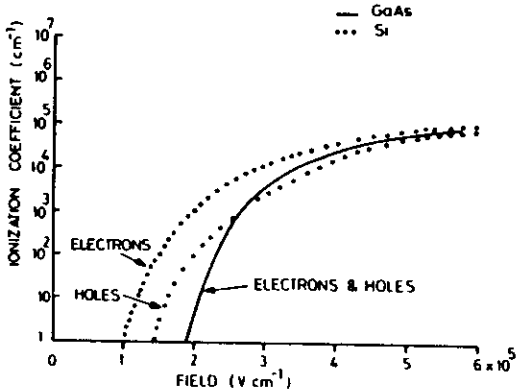

Fig.2.65. Approximate values for the electron and hole ionization coefficients in GaAs and Si at 300K [31]

Material considerations

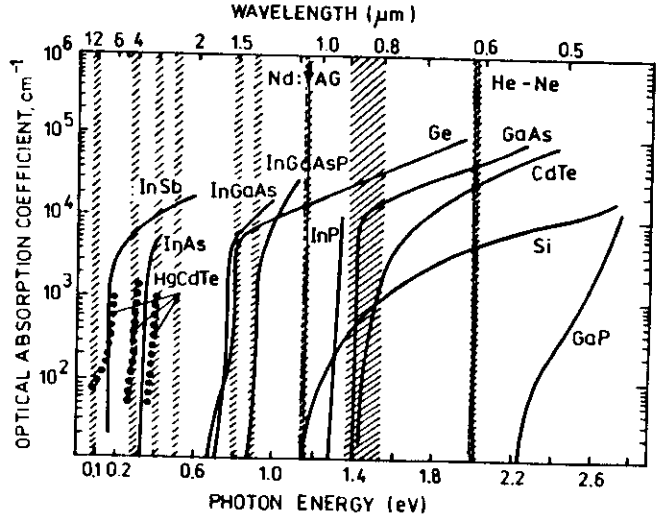

Fig.2.66. Absorption coefficients of the semiconductors important for photodetector technology. The vertical lines and shadowed stripes indicate the Nd : 4 AG and He-Ne laser lines, transmission windows in optical fibres and open athmosphere, respectively

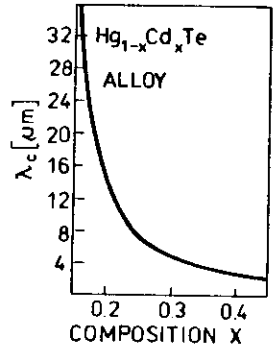

Fig.2.67. Cut-off wavelength as a function of alloy composition for the $Hg_{1-x}Cd_xTe$ alloy [32]

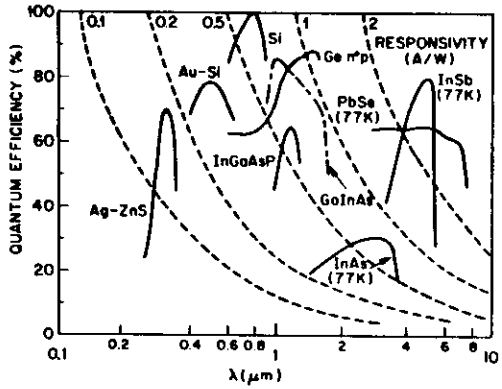

Fig.2.68. Quantum efficiency and responsivity for various photodetectors [26]

HETEROSTRUCTURE PHOTODIODES

Advantages:

- large-bandpag material can be used as a window for the transmission of optical power
- quantum efficiency and response speed can be optimized for a given optical signal wavelength.

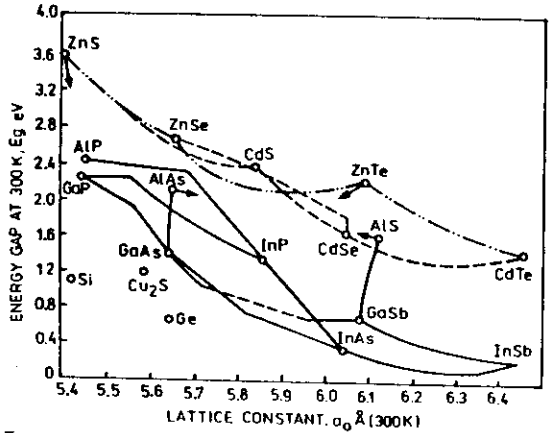

Fig.2.69. Energy gap versus lattice constant for III - V and II - VI compound semiconductors

"Mesa" type photodiodes

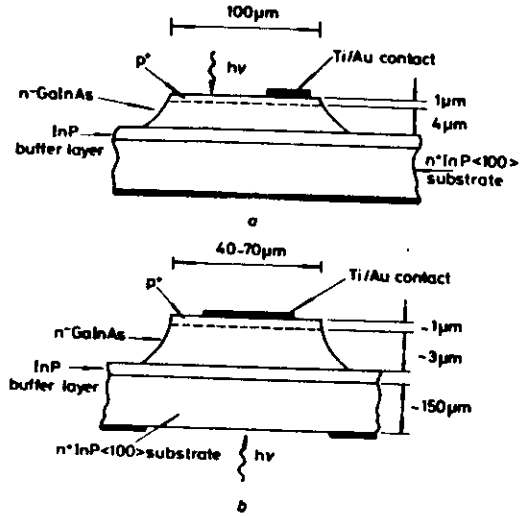

Fig.2.70. Mesa InGaAs/InP PIN photodiodes [34]
a) front-illuminated structure
b) back-illuminated structure

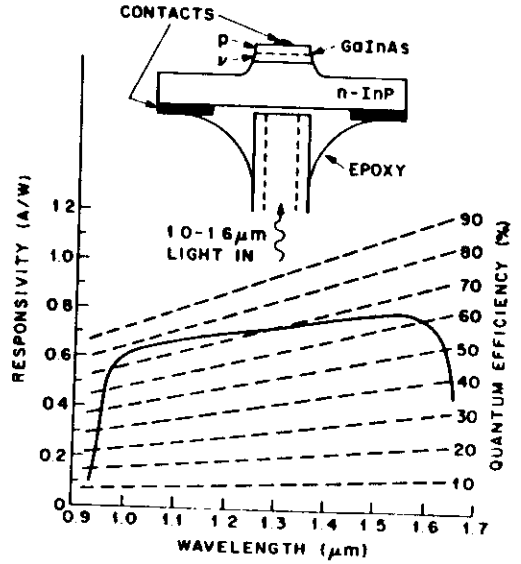

Fig.2.71. Responsivity and quantum efficiency of a InGaAs p-i-n photodiode versus wavelength [35]

Planar photodiodes

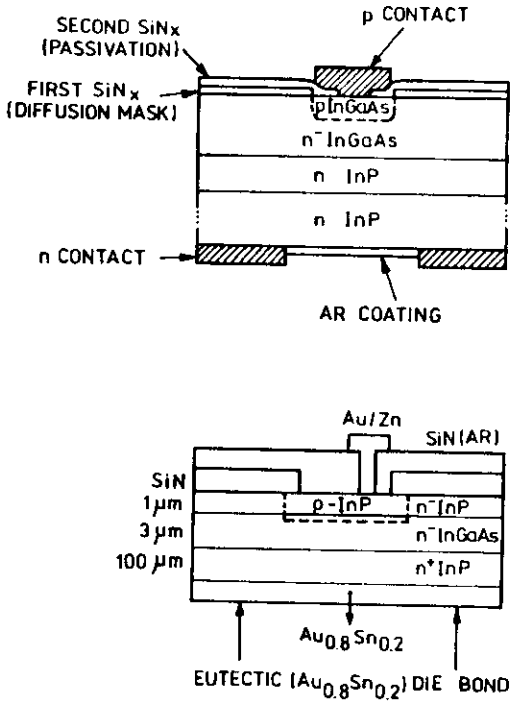

Fig.2.72. Schematics of planar InGaAs/InP photodiodes
a) back illuminated
b) front illuminated

Planar structures are more advanced than mesa types and better suited for large scale production by Chemical Vapor Deposition techniques.

Table 4. Performance Comparison of InGaAs and Ge Detectors (Active Diameter 2 mm; 0 V, 25°C) [41]

	InGaAs	Germanium
Responsivity (A/W)		
1.3 μm	0.8	0.5
1.55 μm	0.9	0.7
0.82 μm	0.2	0.1
Dynamic impedance (kohms)	200	6
NEP ($pW/Hz^{1/2}$)	0.3	2.4
Capacitance (pF)	600	1600
Max. Operating Temperature (°C)	100	60

HETEROSTRUCTURE Avalanche Photodiodes

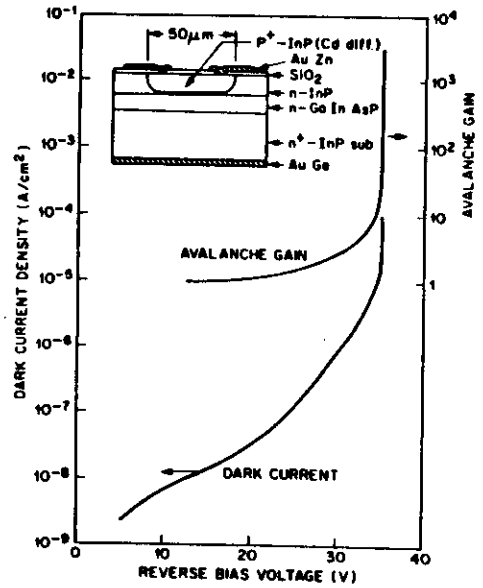

Fig.2.73. Avalanche gain and dark current dependence on reverse bias in a InGaAsP heterostructure avalanche photodiode [36]

"Separate Absorption and Multiplication" concept

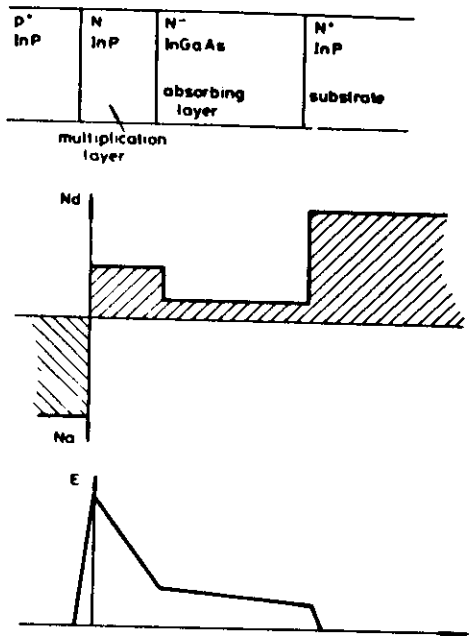

Fig.2.74. Layer composition, doping profile and electric field profile of SAM (separate absorption and multiplication) APD structure

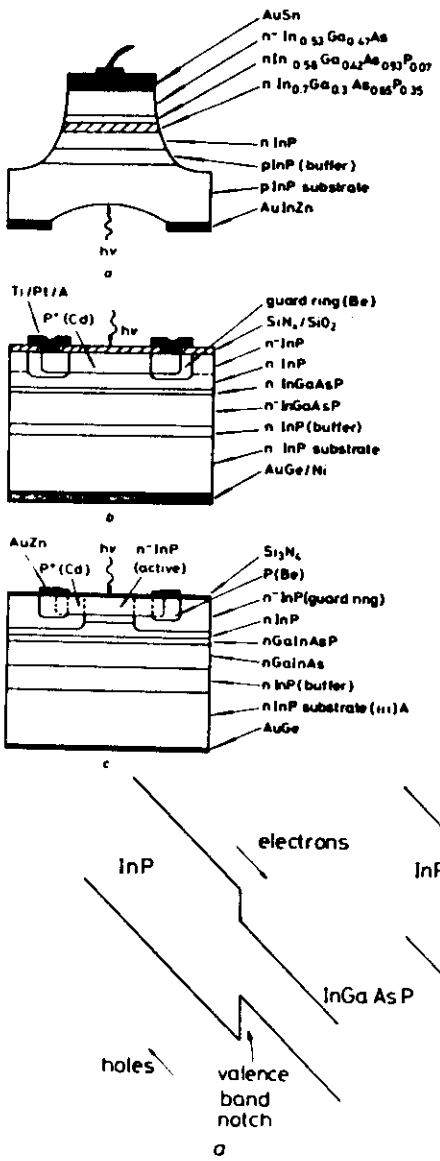

- LPE - grown with p^+ substrate
- VPE - grown with planar structure
- LPE - grown buried structure

Fig.2.75. Recent SAM APD structures [34]

Fig.2.76. Band diagrams of heterostructure APDs a) InP/InGaAs heterojunction showing "notch" in which holes may be trapped, b) InP/InGaAs heterojunction with InGaAsP layer to reduce effect of the "notch"

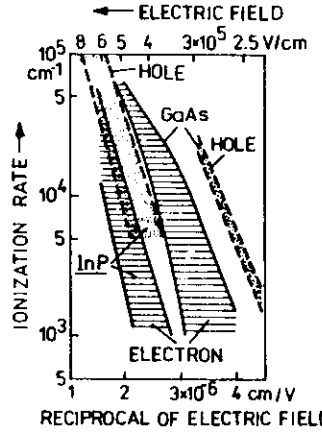

Fig.2.77. Range of measured ionization rates of electrons and holes in InP and GaAs [33]

The ionization coefficient ratio can be artificially enhanced in superlattice APD structures.

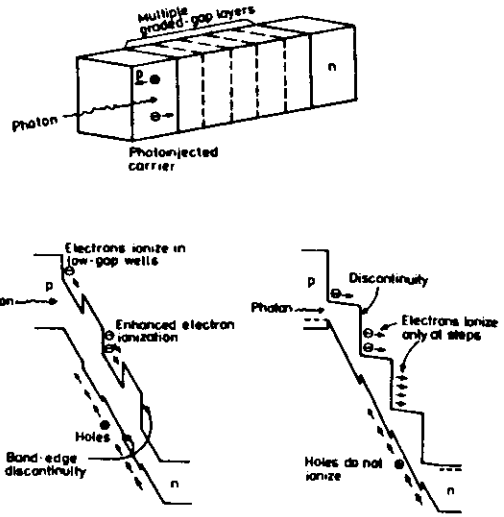

Fig.2.78. Schematic diagram of the superlattice APD; below are shown energy band diagrams of a reverse biased superlattice APD (a) and staircase APD (b) [37]

Table 5. Laboratory measurements of optical receiver sensitivities long-wavelength photodetector types [40]

Type	Bit rate Mb/	Wavelength μm	Normalized receiver sensitivity dBm*	Researchers and year published	Laboratory
Photoconductor					
InGaAs	2000	1.51	-30.3	Chen et al (1985)	AT T Bell Labs
	1000	1.3	-35.9	Chen, Kasper, Cox (1984)	AT T Bell Labs
p-i-n Photodiode					
InGaAs	1200	1.53	-36,6	Smythe et al (1984)	British Telecom Res.
	565	1.3	-40.2	Smith et al (1982)	British Telecom Res.
	447	1.3	-48.8	Ogawa et al (1981)	
APD					
Germanium	2000	1.55	-33.6	Yamada et al (1982)	Nippon Telephone Telegraph Corp. Nippon Electric Corp.
	4000	1.3	-22.0	Takano et al (1985)	
	400	1.3	-38.8	Yamada et al (1978)	
SAM APD					
InGaAs/InP	4000	1.51	-32.7	Kasper et al (1985)	AT T Bell Labs
	420	1.55	-44.3	Kasper et al (1983)	
Integrated detector					
InGaAs p-i-n/ /InP MISFET receiver	100	1.3	-36.0	Kasahara et al (1984)	Nippon Electric Corp.
1 x 12 InGaAs p-i-n array	45	1.3	-40.5	Kaplan, Forrest, Johnson (1986)	AT T Bell Labs
dBm* - decibels below 1 milliwatt of power					

Table 6. Relative merits of fibre optic receivers incorporating III - V PIN diodes, Ge APDs and III - V APDs [34]

	III - V PIN diode	Ge APD	III - V APD
Device structure	simple	difficult especially for 1.55 m operation	very difficult
Fabrication	new technology but relatively simple	established technology	still in research stage, yields poor
Receiver sensitivity	very good at low bit rates progressively worse above 565 Mbit/s trade off with dynamic range	better at high bit rates, especially if device cooled	potentially gives best sensitivity, but by only a few dB. Still considerably inferrior to Si APD
Associated circuity	low voltages, high performance FETS needed great care with circuit layout to minimise stray capacitances	high voltage operation simpler circuity, but more of it, extra circuity to stabilise gain, and compensate for temperature variations	
Applications	chosen for submarine systems because of simplicity, will be preferred for coherent systems	preferred for bit rate land systems at present problems with saturation in coherent systems	still at research stage

Table 7. Properties of infrared quantum detectors

Material	Wavelength range [μm]	Operating temperature [K]	Peak detectivity 10^{10} [cm $Hz^{1/2}$ W^{-1}]	Response time [μs]
Ge	0.8 - 1.8	295	10	0.001 - 0.2
PbS	1 - 2.5 1 - 3.3	295 77	8 - 15 15 - 25	250 5000
InAs	2.3 - 3.8 1.3 - 3.2	295 77	0,5 40	0.1 1
InSb	1.5 - 5.3	77	10 - 40	0.1 - 1
CdHgTe	3 - 5	295 195 77	0.2 - 0.5 2 - 10 5 - 10	0.005 - 10 0.2 - 1 10
CdHgTe	8 - 13	77	0.5 - 3 0.5 - 2	0.2 - 1 0.001 - 0.1
CdHgTe	10 - 22	77	1	0.2

PHOTOTRANSISTORS

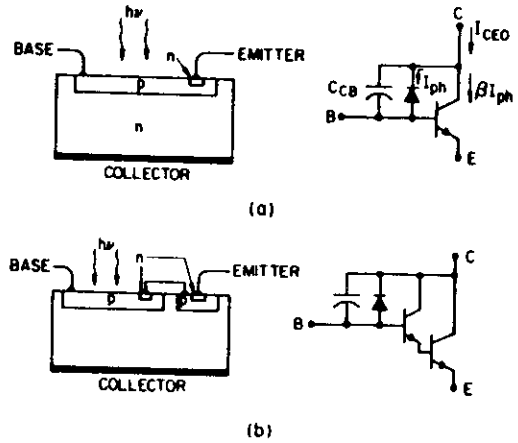

Fig.2.79a) Bipolar phototransistor, b) Photo - Darlington[38] Characteristic feature: large base-collector junction serving as the light-collecting element. Effective quantum efficiency is $(1 + h_{FE})$ times larger than that of the base-collector photodiode. Frequency response limited by large C_{CB} and by the gain of the detector due to feedback effect ($\tau_r \geq 5\,\mu s$)

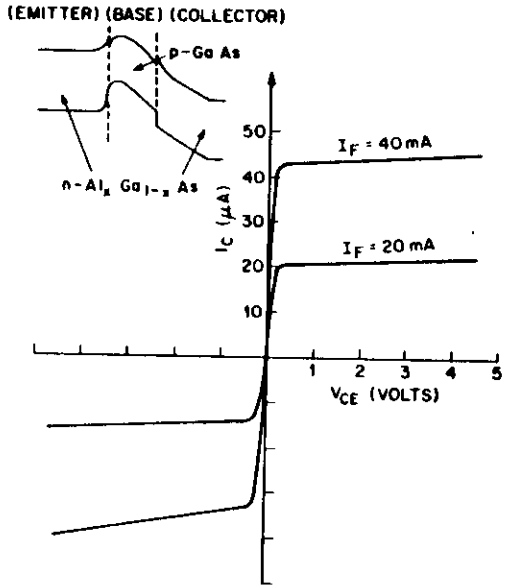

Fig.2.80. Current-voltage characteristics of a bilateral symmetrical heterostructure phototransistor [39]

2.3. OPTO-COUPLERS (OPTO ISOLATORS) [26] [42], [43]

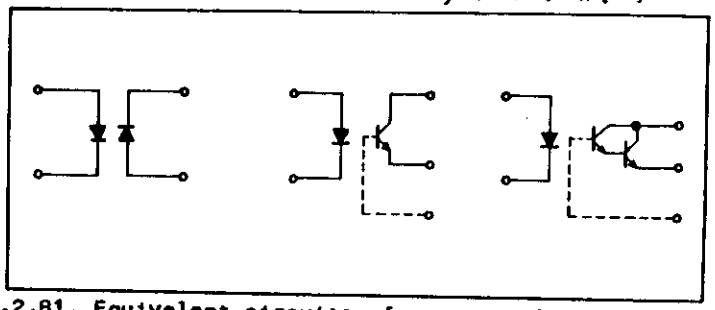

Fig.2.81. Equivalent circuits of opto-couplers

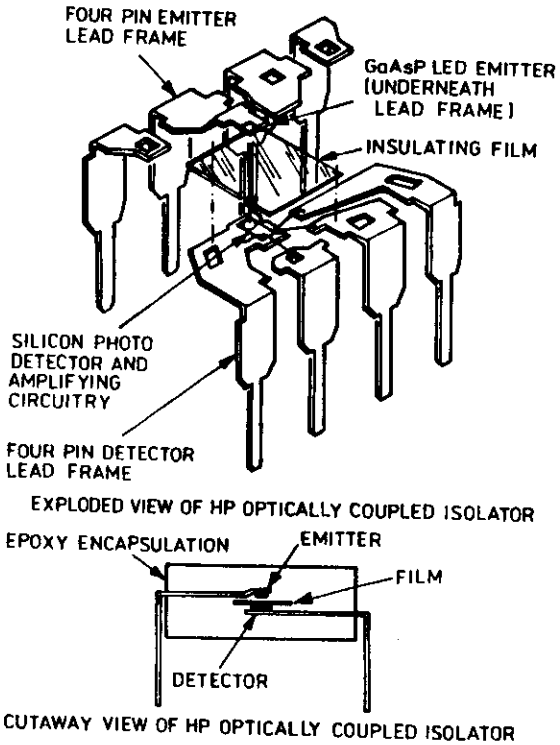

Fig.2.82. Mechanical construction of plastic encapsulated opto-couplers. The GaAs (or GaAsP) emitter and silicon detector are die attached and wire bonded to separate four-pin lead frames. An isulating film is sandwiched between the emitter and detector lead frames

other constructions : reflection opto-couplers

Table 8. Typical parameters of currently manufactured opto-couplers [44]

Features	Typical Data Rates	Current Transfer Ratio	Input current	Input T_o Output Insulation
General Purpose, Photo-transistor output	Rise/Fall Time 0.3µs	30%	60 mA	2500 V
High Speed Transistor Output	1 Mbit/s	7%	16 mA	3000 V
Ultra High Speed Optically Coupled Logic	10 Mbit/s	600%	5 mA	3000 V
Low Input Current, High Gain	300 kbit/s	300%	1.6 mA	3000 V

3. FUTURE TRENDS

In optical communication : longer wavelengths

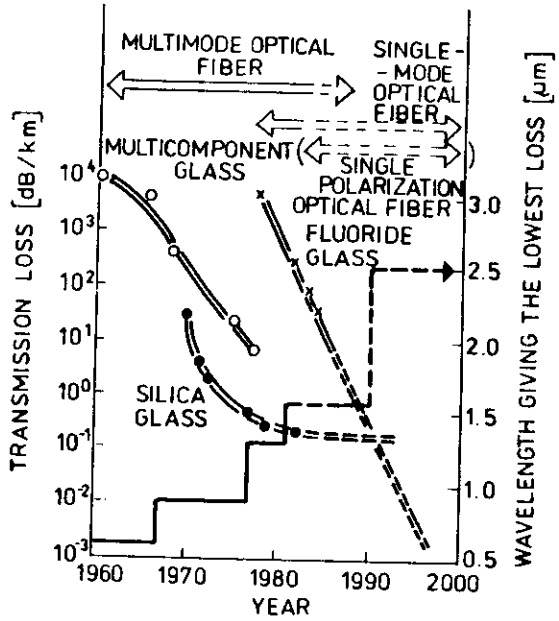

Fig.3.1. Progress of optical fibres and their future progress. By the 1990s development of infrared transmission material will decrease the optical fibre transmission loss below silica glass's theoretical limit at a 2 - 4 μm wavelength, causing an increase of demand for single-mode fibre [45]

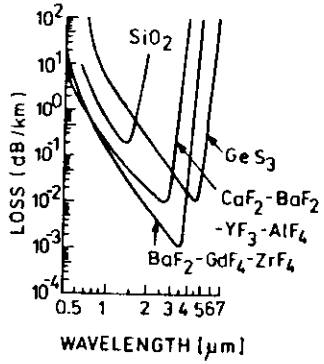

Fig.3.2. Estimate of loss for infrared materials [46]

New semiconductors are being tested:

- GaInAsSb/InAs
- GaInAsSb/GaSb
- InAsSbP/InAs
- AlGaAsSb/GaSb

- In optical information processing : shorter wavelengths towards visible

Solution : quantum well lasers (QW)

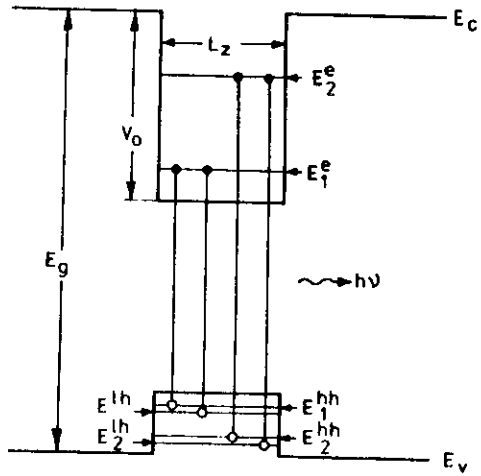

Fig.3.3. Energy level diagram of confined electrons and holes together with the allowed radiative transitions (n = 0). Higher energy levels contribute to short wavelength lasing

- In general : higher CW output power
higher speed of modulation

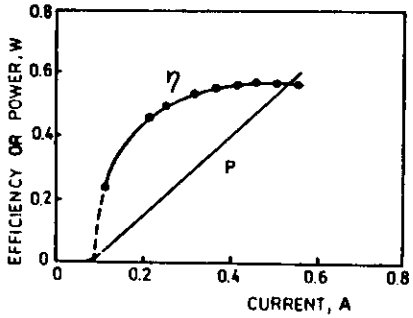

Fig.3.4. Output power and power-conversion efficiency as a function of supply current. Single-stripe laser emits more than 0.5 W of 0.826 m light while operating at a power--conversion efficiency of 57% [47]

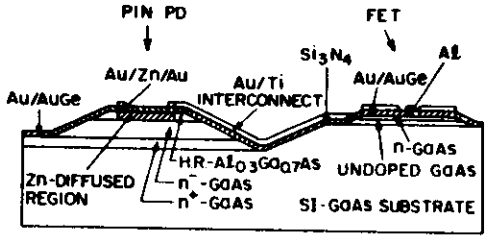

(a)

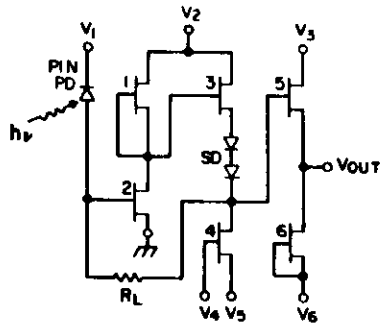

(b)

Fig.3.5. An integrated receiver consisting of a p-i-n photodiode and a field-effect transistor preamplifier designed for operation at short wavelengths (0.8 to 0.9 μm) [48]. Such integrated receivers have been tested in the laboratory, but fabrication difficulties have not get been surmounted for actual systems

4. BIBLIOGRAPHY

1. Y. Horikoshi: in Semiconductors and Semimetals, vol.22, Part C ed.W.T.Tsang Academic Press. mc., 1985 , p.93.

2. H. Kressel, J.K. Butler: Semiconductor Lasers and Heterojunction LEDs Academic Press, New York, 1977 .

3. H. Kressel et al: Semiconductor Devices for Optical Communication Springer-Verlag, Berlin, Heidelberg, New York, 1980 .

4. H.C. Casey Jr., M.B. Panish: Heterostructure Lasers Academic Press, New York, 1978 .

5. R.C. Goodfellow, R. Davis: in Optical Fibre Communications, Devices, Circuits and Systems, eds. M.J. Howes, D.V. Morgan, John Wiley and Sons, Chichester 1980 .

6. H. Temkin, V.G. Keramidas: J.Appl.Phys. vol.51, 1980 , p.3269.

7. D.E. Aspnes: Surface Science, vol.132, 1983 , p.406.

8. Y. Suematsu: Proc. IEEE, vol.71, No 6, 1983 , p.692.

9. D. Botez, G.J. Herskowitz: Proc. IEEE, vol. 68, 1980 , p. 689.

10. R.L. Moon, G.A. Antypas, L.W. James: J. Electronics Mater. vol. 3, 1974 , p. 635.

11. J.I. Pankove, H. Kressel: Israel J. of Technology, vol. 9, 1971 , p. 221-231.

12. R. Chin, N. Holonyak, Jr. B.A. Vojak, K. Hess, R.D. Dupuis, P.D. Dapkus: Appl.Phys.Letters, vol. 36, No 1, 1980 , p. 19-21.

13. D. Botez: IEEE Spectrum, vol. 22, No 6, 1985 , p. 43.

14. K. Aiki, M. Nakamura, T. Kuroda, J. Umeda, R. Ito, N.Chinone, M. Maeda: IEEE J. Q. El., vol. QE-14, 1978 , p. 89.

15. D. Botez: Appl. Phys. Lett., vol. 36, No 3, 1980 , p. 190.

16. D.R. Scifres, R.D. Burnham, W. Streifer: Appl. Phys. Lett., vol. 41, 1982 , p. 118.

17. D. Botez, D.E. Ackley: IEEE Circuits and Devices Magazine, vol. 2, No 1, 1986 , p. 8.

18. N. Yoshikawa, K. Itoh, G. Kano, I. Teramoto: IEEE J. Q. El. vol. 21, No 6, 1985 , p. 623.

19. H.C. Casey Jr., M.B. Panish, J.L. Merz: Appl. Phys. Lett., vol. 44, 1973 , p. 5470.

20. Y. Uematsu, H. Okuda, J. Kinoshita: Electron. Lett., vol. 18, No 20, 1982 , p. 857.

21. K. Utaka, K. Kobayashi, Y. Suematsu: J. Quantum Electron. vol. QE-17, No 5, 1981 , p. 651.

22. W.T. Tsang, N.A. Olsson, R.A. Logan: Appl. Phys. Lett., vol. 42, No 8, 1983 , p. 650.

23. J.P. van der Ziel, R.M. Mikulyak: IEEE J. Quantum Electron., vol. QE-20, No 3, 1984 , p. 223.

24. T.E. Bell: IEEE Spectrum, vol. 20, No 12, 1983 , p.38.

25. H. Preier, R. Grisar: Measurement, vol. 3, No 4, 1985 , p. 153.

26. S.M. Sze: Physics of Semiconductor Devices, John Wiley and Sons 1981 , p. 743.

27. E.L. Dereniak, D.G. Crowe: Optical Radiation Detectors, John Wiley and Sons, 1984 .

28. H. Melchior: in Laser Handbook, vol. 1, eds. F.T. Arecchi and E.O. Schulz-Dubois, North Holland, Amsterdam 1972 , p. 725-835.

29. M.V. Schneider: Bell Syst. Tech. J., vol. 45, 1966 , p. 1611.

30. H. Melchior, A.R. Hartman, D.P. Schinke, T.E. Seidel: Bell Syst. Tech. J. vol. 57, No 6, 1978 , p. 1791-1807.

31. D.R. Wight: in Gallium Arsenide, ed. M.J. Howes, D.V. Morgan, John Wiley and Sons, 1985 , p. 21.

32. M.A. Herman, M. Pessa: J. Appl. Phys., vol. 57, 1985 , p. 2671.

33. A. Schlachetzki: Archiv für Elektronik und Übertragungs-technik, vol. 40, No 5, 1986 , p. 302.

34. D.H. Newmann, S. Ritchie: IEE Proc., vol. 133, No 3, 1986 p. 213.

35. T.P. Lee, C.A. Burrus, A.G. Dentai: IEEE J. Quantum Electron., QE-17, 1981 , p. 232.

36. K. Nishida, K. Taguchi, Y. Matsumoto: Appl. Phys. Lett., vol. 35, 1979 , p. 251.

37. F. Capasso: Surface Science, vol. 132, 1983 , p. 527.

38. J.S. Jayson, S. Knight: in Applied Solid Science, vol. 6, ed. R. Wolfe Academic, New York, 1976 , p. 119-168.

39. S. Knight, L.R. Dawson, V.G. Keramidas, M.G. Spencer: IEEE Tech. Dig. Int. Electron Device Meet. 1977, p.472.

40. S.R. Forrest: IEEE Spectrum, vol. 23, No 5, 1986 , p. 76.

41. G.H. Olsen, V.S. Ban: Solid State Technology, vol. 30, No 2, p. 99.

42. S. Gage, D. Evans, M. Hodapp, A. Sorensen: in Optoelectronics Applications Manual Mc Graw-Hill Book Co., New York, 1977 .

43. A. Chappell editor : Optoelectronics Theory and Practice Mc Graw-Hill Book Co., New York, 1978 .

44. Optoelectronics Devices Catalogues

45. Y. Takeda, H. Yoshine, Y. Koga, M. Maeda: Hitachi Rev., vol. 33, No 4, 1984 , p. 167.

46. S. Schibata, M. Horiguchi, K. Jinguji, S. Mitachi, T. Kanamori, T. Manabe: Electron Letter, vol. 17, No 12, 1981 , p. 775.

47. Editorial: Laser Focus/Electro-Optics, March, 1987 , p.24.

48. O. Wada, T. Sakurai, T. Nakagami: J. Quantum Electron., vol. QE-22, No 6, 1986 , p. 805.